AD 871989

AUTHORITY: DWTNSRDC
ltr, dtd 2 Mar 84

NAVAL SHIP RESEARCH AND DEVELOPMENT CENTER

Washington, D.C. 20034

THE EFFECT OF RESIDUAL STRESSES ON THE BUCKLING STRENGTH OF FABRICATED HY-80 STEEL HEMISPHERICAL SHELLS

by

M.G. Costello

STRUCTURAL MECHANICS LABORATORY

RESEARCH AND DEVELOPMENT REPORT

October 1970

Report 3407

REPORT 3407

EFFECT OF RESIDUAL STRESSES ON THE BUCKLING STRENGTH OF FABRICATED HY-80 STEEL HEMISPHERICAL SHELLS

The Naval Ship Research and Development Center is a U.S. Navy center for laboratory effort directed at achieving improved sea and air vehicles. It was formed in March 1967 by merging the David Taylor Model Basin at Carderock, Maryland and the Marine Engineering Laboratory (now Naval Ship R & D Laboratory) at Annapolis, Maryland. The Mine Defense Laboratory (now Naval Ship R & D Laboratory) Panama City, Florida became part of the Center in November 1967.

Naval Ship Research and Development Center
Washington, D.C. 20034

MAJOR NSRDC ORGANIZATIONAL COMPONENTS

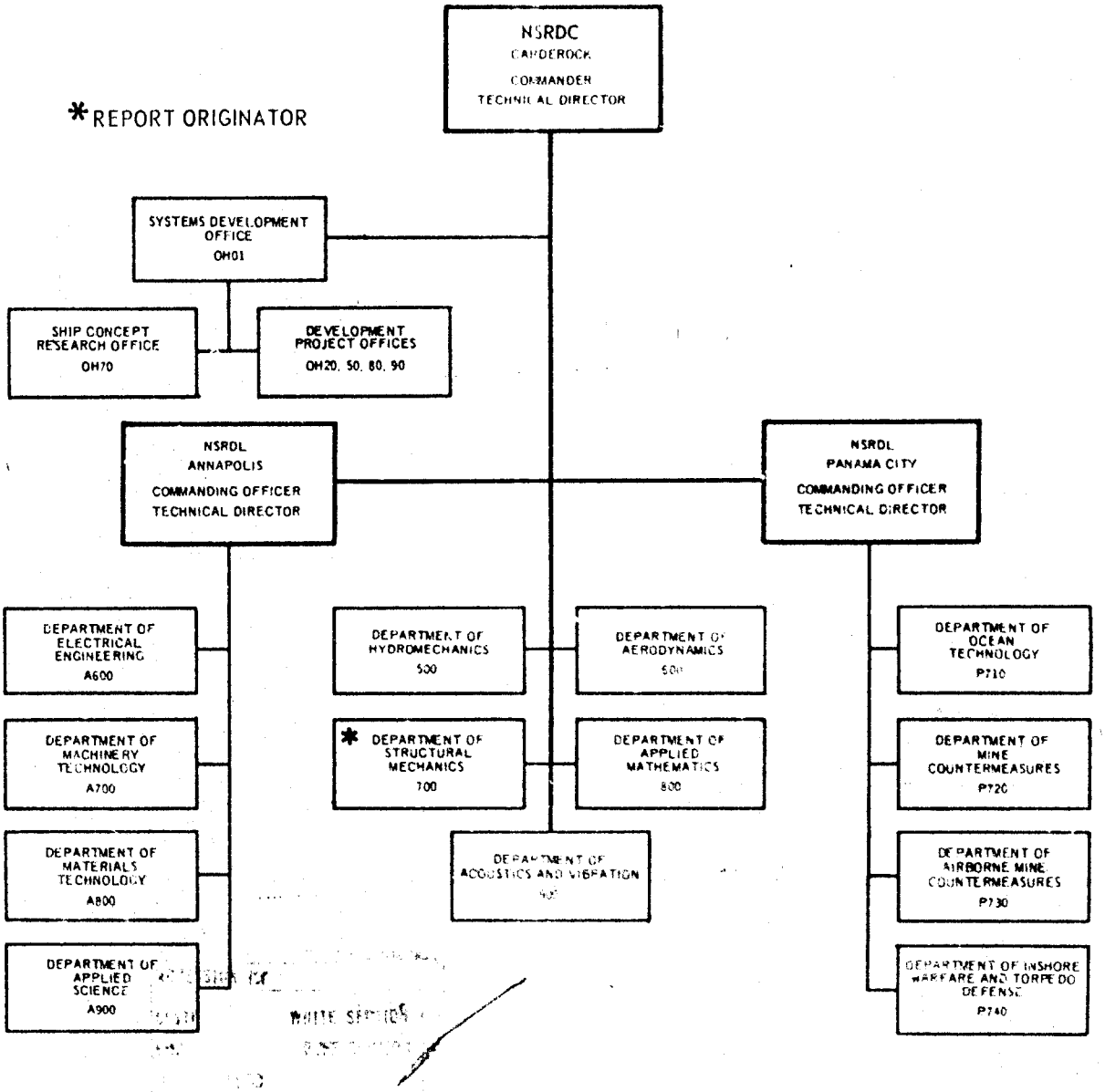

DIST. 2

DEPARTMENT OF THE NAVY
NAVAL SHIP RESEARCH AND DEVELOPMENT CENTER
WASHINGTON, D.C. 20034

THE EFFECT OF RESIDUAL STRESSES ON THE BUCKLING STRENGTH OF FABRICATED HY-80 STEEL HEMISPHERICAL SHELLS

by

M.G. Costello

October 1970 Report 3407

TABLE OF CONTENTS

LIST OF FIGURES

LIST OF TABLES

ABSTRACT

Hydrostatic tests were conducted on nine fabricated HY-80 steel hemispheres to observe the effects of residual stresses from cold forming and welding on elastic response and collapse strength. Nondimensionalized collapse data indicated that residual stresses due to welding play a significant part in the collapse strength of fabricated HY-80 steel hemispheres.

ADMINISTRATIVE INFORMATION

The work described in this report was sponsored by the Naval Ship Systems Command, Subproject SF 35.422.210, Task 15054.

INTRODUCTION

For several years the Naval Ship Research and Development Center (NSRDC) has been studying realistically fabricated hemispherical shells in order to determine the individual contributions of such factors as local flat spots and thin spots, mismatch at joints, residual stresses, and boundary conditions to the observed reduction in strength of these shells as compared with perfect hemispheres. Tests have been conducted on both 30- and 66-in. diameter HY-80 hemispheres fabricated by welding together six doubly curved "orange peel" shell segments plus a shallow polar cap. Some of these hemispheres were hydrostatically tested in the as-fabricated condition while others were stress relieved prior to hydrostatic testing. Comparison of test results[1,2] indicated an appreciable difference in collapse strengths attributable to the weakening effects of residual stresses, first from cold forming the individual segments and second from welding the segments together. Since forming stresses can be eliminated on prototype hulls by stress relieving the segments or by using hot forming practices, the project herein reported was initiated to determine the effect of welding residual stresses alone.

Seven 66-in. diameter and two 30-in. diameter hemispheres were fabricated and tested. Of the 66-in. diameter hemispheres, three, AF-1,

---

[1] References are listed on page 51.

AF-2, and AF-3, were tested in the as-fabricated (cold formed) condition while the segments for the other four, SRS-1, SRS-2, SRS-3, and SRS-4, as well as the two 30-in. diameter hemispheres SRS-2A and SRS-3A, were stress relieved after light tack welding and before final welding. The as-fabricated models were made to supplement previous test data.

DESCRIPTION OF MODELS

Seven 66-in. diameter HY-80 steel hemispheres were made by the Lukens Steel Company using procedures used for full-scale submarine bulkheads. Except where noted, the methods were the same as used for the 66-in. diameter hemispherical models reported in References 1 and 2. Each of the present models consisted of six 60-deg "orange peel" segments and one shallow spherical cap, all formed from pieces of the same flat plate. An assembled hemisphere is shown in Figure 1. Models AF-1, AF-2, and AF-3 were made by cold forming the individual segments and welding them together. Models SRS-1, SRS-2, SRS-3, and SRS-4 were made by hot forming the individual segments, lightly tack welding them in place, stress relieving for an hour at 1025 deg, and finally welding the segments.

Models SRS-2A and SRS-3A, 30-in. diameter HY-80 hemispheres, were made at NSRDC. The segment configuration was the same as for the 66-in. diameter hemispheres. The individual segments were cold formed, lightly tacked to their mold and stress relieved at 1025 deg for an hour. The stress relieved segments were then welded together.

In the case of the two 30-in. models, SRS-2A and SRS-3A, two extra "orange peel" segments were cut from the same plates and cold formed. Compression specimens were cut from one segment. The other segment was stress relieved with its model after which compression specimens were taken. The yield strength distribution for these extra segments is shown in Figure 2. Typical stress-strain curves for model SRS-2A from the original flat plate and the two extra formed segments are shown in Figure 3.

For all calculations Young's modulus and Poisson's ratio were assumed to be 30×10^6 psi and 0.3, respectively. For all models the yield strength σ_y of the original plate was used in calculations for the collapse pressure. It is realized that this will not be representative of the

material in place for the three AF models because of work hardening. Data on the variation in yield strength due to forming and stress relieving is presented in Table 1.

Prior to testing each hemispherical model was welded to a stiffened cylinder. The cylinders used on the 66-in. and 30-in. hemispheres were made from HY-80 and HY-150 steel respectively for two previous series of hemispheres. Although the cylinders did not provide membrane boundaries at the hemisphere-cylinder juncture, it was felt that the stiffnesses would be sufficiently close to preclude any detrimental effects. Model and cylinder assemblies are shown in Figure 1 together with nominal dimensions.

PROCEDURE

DETERMINATION OF INITIAL IMPERFECTIONS

The analysis for imperfect spherical shells[3] requires the determination of local imperfections over the entire shell surface. This was accomplished by measuring deviations from an assumed radius using an assumed center as reference. This data was fed into a computer program, YL01, which calculated a new center and new average radius and modified the deviations accordingly. These deviations were plotted in the form of contour maps as shown in Figure 4. Minus signs indicate inward deviations. The view is of the inside of the model rolled out into a flat surface whose radial scale remains constant. The scale factor is found by dividing one half of the circumference of the hemisphere by the diameter of the plotted circle. The scale in all other directions is a function of orientation and distance from the center of the plot. To overcome the mapping problem clear plastic overlays such as shown in Figure 5 were used. Any diagonal across an oval represents the same arc length on the hemisphere.

In addition to sphericity readings 151 thickness readings were made on each shell. They are presented in Table 2.

The contour map, overlay, and thickness table were used to examine flat spot areas. The method is described in detail in References 1 and 3. Each flat spot was characterized by its ratio of local to nominal radius R_1/R and its local thickness h_a.

In addition to flat spots, mismatches at welded joints in terms of deviations from sphericity are given in Figure 4.

Recently the examination of flat spots has been automated. A computer program, OSR1, written by R.D. Rockwell of NSRDC incorporates YL01 but requires the additional input of thickness measurements. Output includes the contour map which was heretofore plotted by hand and a table of local radii.

TEST PROCEDURE

Each hemisphere was instrumented with between 50 and 150 foil-resistance strain gages. Areas for gaging were chosen on the basis of flat spot calculations and mismatch readings. Additional gages were placed at the edges of segments for the SRS models to detect the effect of welding residual stresses. Strain gage locations are shown in Figure 6.

The 66-in. and 30-in. models were statically tested in oil in the NSRDC 6-foot head testing tank and 4-foot testing tank, respectively. The test setup is shown in Figure 7. In most cases each test consisted of three pressure runs--the first and second to approximately 70 and 90 percent, respectively, of the collapse pressure and the third to collapse. The final increment prior to collapse was less than 2 percent of the collapse pressure.

RESULTS AND DISCUSSION

Experimental collapse pressures for each model are shown in Table 3. Figure 6 shows strain sensitivities defined by the slope of the initial linear portion of the applied pressure versus measured strain curve and given in μin./in./psi.

Typical pressure-strain plots are presented in Figure 8. Pressure-strain data for Model SRS-1 is not available for presentation. For such an unstable model it is unlikely that strain gages at local flat spots experienced appreciable nonlinearity prior to collapse. Model SRS-2 is also not included. For this model all gages were linear up to collapse. Figure 9 shows the models after collapse.

Nondimensional plots of experimental results for the nine models are presented in Figure 10; the abscissa is the ratio of elastic buckling pressure P_3' to the yield pressure P_y', and the ordinate is the ratio of the experimental collapse pressure P_c to P_y'. It should be noted that local geometry in the area of failure was used to calculate P_3' and P_y', which are defined by the expressions

$$P_3' = 0.84E\left(\frac{h_a}{R_{10}}\right)^2 \quad \text{for } \nu = 0.3 \tag{1}$$

$$P_y' = \frac{2\,\sigma_y\,h_a\,R_{1m}}{(R_{10})^2} \tag{2}$$

where h_a is the average thickness at the flat spot,
R_{10} is the local outside radius,
R_{1m} is the local midsurface radius,
E is Young's modulus, and
σ_y is the yield strength.

Results of References 1 and 2 have been included for comparison. The difference between the yield line and the lower bound for the stress relieved models of References 1 and 2 was attributed to secondary moments. The difference between the lower bounds for the previous stress relieved models and the present models composed of stress relieved segments (SRS) is attributed to residual welding stresses. The difference between the lower bounds for the SRS models and the models tested in the as-fabricated (AF) state is attributed to residual forming stresses. The present results for the three as-fabricated models are consistent with previous results. The data point for AF-2 lies on the previously determined lower bound curve for as-fabricated hemispheres. AF-2 failed near a meridional weld. The data points for AF-1 and AF-3 however are considerably above the lower bound line. These two models failed in the middle of "orange peel" segments. A certain amount of scatter is evident in the data points for the six models composed of stress relieved segments. SRS-3A for example proved stronger than a comparable hemisphere without residual welding

stresses. The lower bound curve for these six models is somewhat lower than one might expect. It appears that removing the residual forming stresses does not do as much to increase the buckling pressure as does removing the residual welding stresses. The failure areas for all but SRS-4 of these six models were near welded joints.

Local fabrication mismatch between adjoining segments of the 66-in. diameter hemispheres was 0.1 inch or less. Mismatch for the 30-in. diameter hemispheres was 0.04 inch or less. This amounted in some cases to as much as 26 percent of the shell thickness. Although this sounds excessive it should be mentioned that the severity of the mismatch was always limited to a fraction of the length of the connection. None of the most severe mismatches as shown in Figure 4 are within the failure areas. The effect of mismatch alone on the collapse strength of hemispherical shells has been investigated and the results presented in Reference 4.

As is readily apparent from Table 4 only three of the nine models of this series collapsed at area I, the geometrically "critical" area based on minimum h_a/R_1. This is attributed to such factors as variations in residual stress, yield strength, the shape of the stress-strain curve and the shape of the flat spots which are neglected in the present analysis. Prior to destructive testing one must assume that failure will occur at area I. The predicted collapse pressure, P_{pred}, is thus based on the local geometry of area I. Should failure occur at a less "critical" flat spot the analysis becomes more conservative. Table 4 shows values of P_{pred} for the present series of models and compares them with the experimental collapse pressures P_{exp}.

Although both areas I and VI were within the failure area of SRS-2, area VI was used for the collapse calculations for two reasons. First, area VI was the closest to the center of the failure area and second, no nonlinearity of strains was recorded at area I just prior to failure. Because of its relatively low R_1/R ratio no strain gages were placed at area VI.

Measured maximum membrane stress sensitivities are compared with their theoretical or calculated counterparts at several flat spot areas for each model in Table 3. Equations defining the two stress sensitivities are also given in the table. With few exceptions agreement between the

two was within 10 percent with the calculated value usually greater than the measured value. Looking at the exceptions in Table 3 in all but one case, SRS-3 area V where all measured strain sensitivities were somewhat suspect, the calculated stress was higher than the measured value.

CONCLUSIONS

1. Residual welding stresses appear to play a significant role in the collapse strength of HY-80 steel hemispheres. Nondimensionalized collapse data for hemispheres whose formed segments had been stress relieved prior to being welded together fell closer to the lower bound results for hemispheres tested in the as-fabricated condition than to the lower bound for completely stress relieved hemispheres.

2. The agreement between calculated and measured membrane stress sensitivities at flat spot areas was fairly good. With few exceptions agreement was within 10 percent.

ACKNOWLEDGMENTS

The major contributions of Mr. K. Nishida during the course of this project are acknowledged. The continued interest and suggestions of Messrs. M.A. Krenzke and T.J. Kiernan are appreciated. The support of Mr. R.M. Charles in directing the fabrication, instrumentation, and testing of the models is also acknowledged.

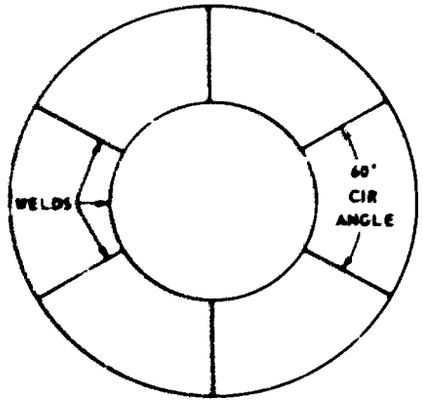

MODEL	a	b	c	d	e	f	g	h_a	i	k	m	n
AF-1	2 3/8	5/8	1/2		1/2	1 1/2	65	3/8	2 1/2	66		
AF-2	3	1	13/16		13/16	2	64 13/16	17/32	2 1/4	66		
AF-3	3	1	13/16		13/16	2	64 13/16	23/32	2 1/4	66		
SRS-1	2 3/8	5/8	1/2		1/2	1 1/2	65	1/4	2 1/2	66		
SRS-2	2 3/8	5/8	1/2		1/2	1 1/2	65	3/8	2 1/2	66		
SRS-3	3	1	13/16		13/16	2	64 13/16	17/32	2 1/4	66		
SRS-4	3 1/4	1 1/4	1 1/8		1 1/8	2 1/2	64 5/8	23/32	3 3/4	58 1/2		
SRS-2A	0.95	0.51	0.16	9.50	0.24	0.38	29.64	0.16	0.67	30.0	0.15	0.13
SRS-3A	1.20	0.65	0.30	0.82	0.42	0.55	29.44	1/4	1.00	30.0	0 25	0.20

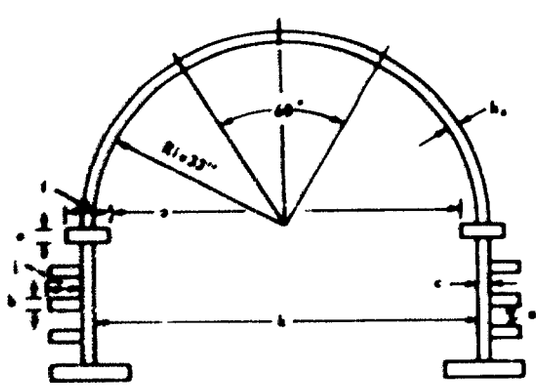

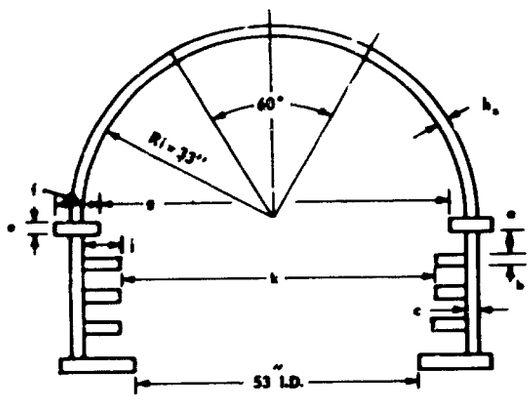

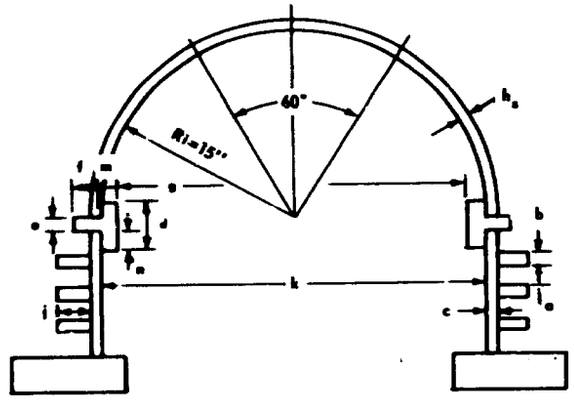

Figure 1 - Model and Cylinder Assembly

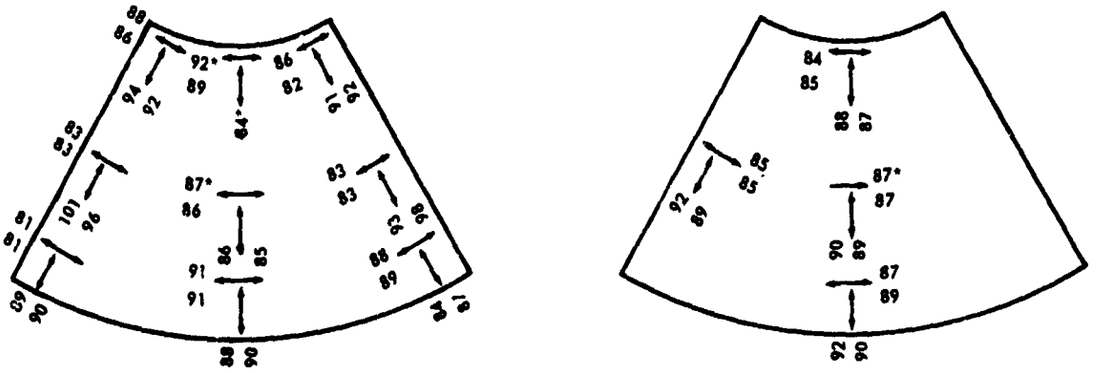

AS FABRICATED

STRESS RELIEVED

SRS-2A

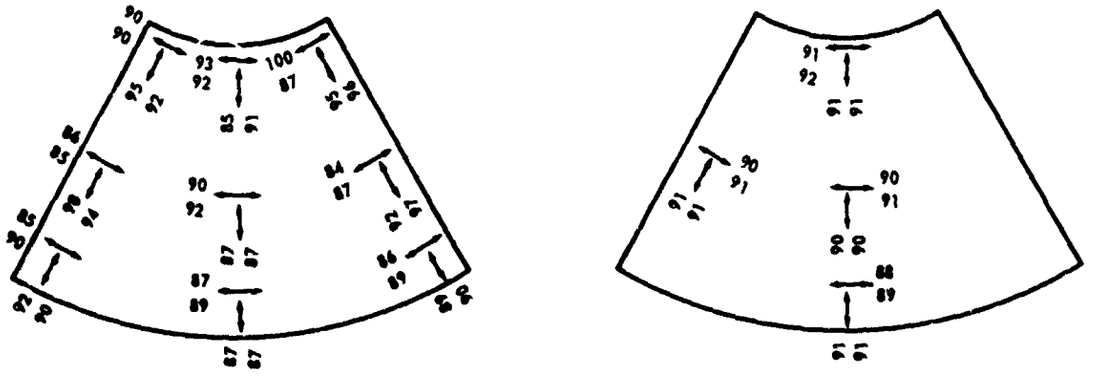

AS FABRICATED

STRESS RELIEVED

SRS-3A

0.2 PERCENT YIELD STRENGTHS ARE IN KSI.
* PLOTTED IN FIGURE 3

Figure 2 - Yield Strength Distribution in As-Fabricated and Stress Relieved Formed Segments for Models SRS-2A and SRS-3A

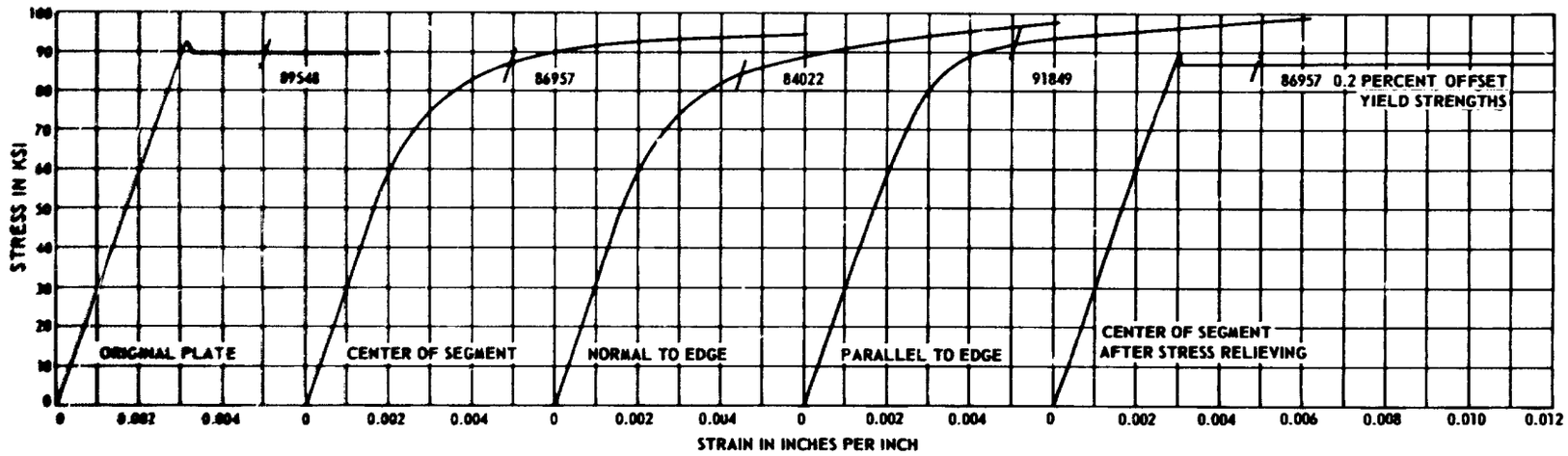

Figure 3 - Typical Stress-Strain Curves from Original Plate, Segment after Forming, and Segment after Forming and Stress Relieving of Model SRS-2A

Figure 4 - Deviations from Sphericity

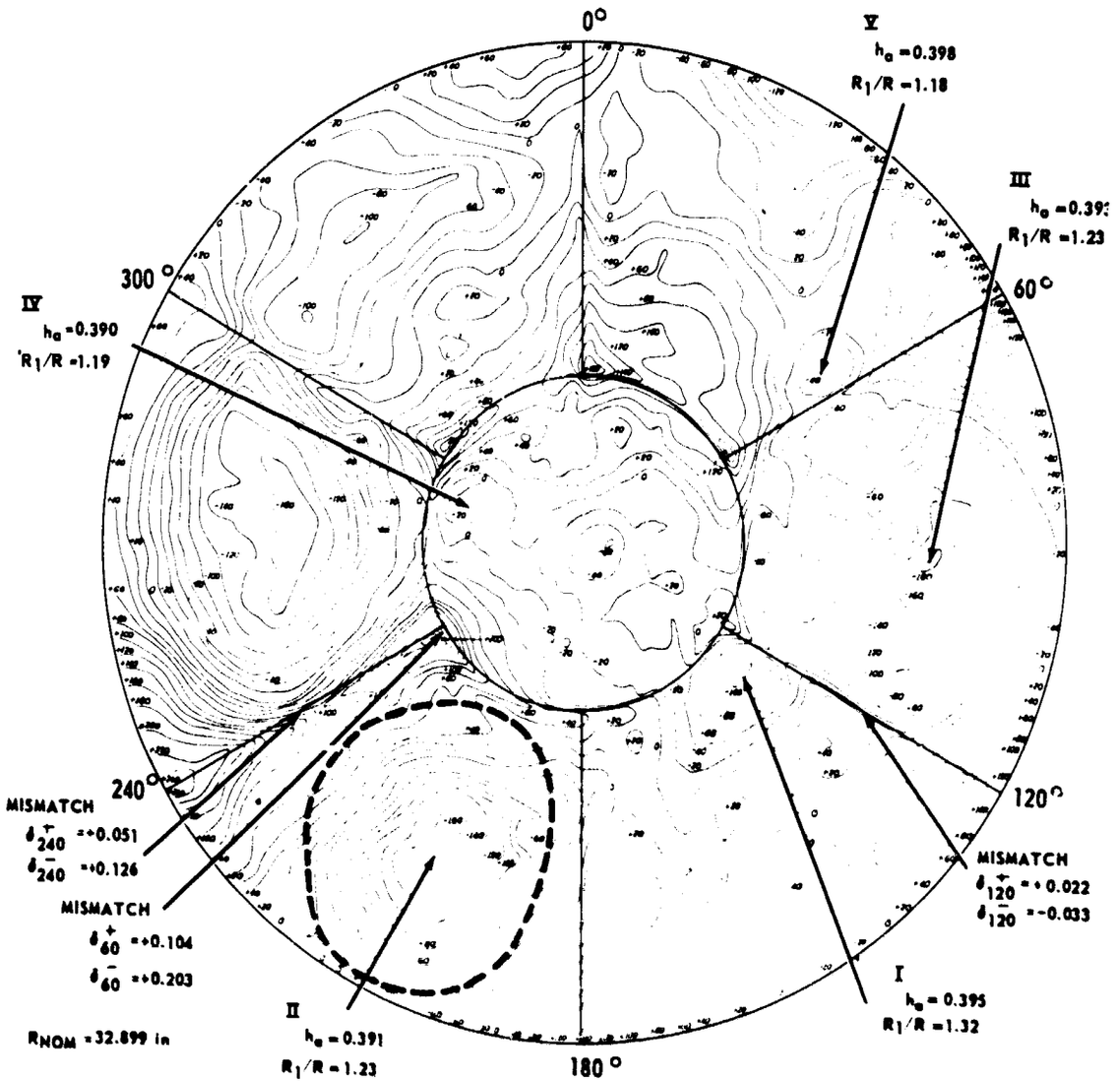

Figure 4a - Model AF-1

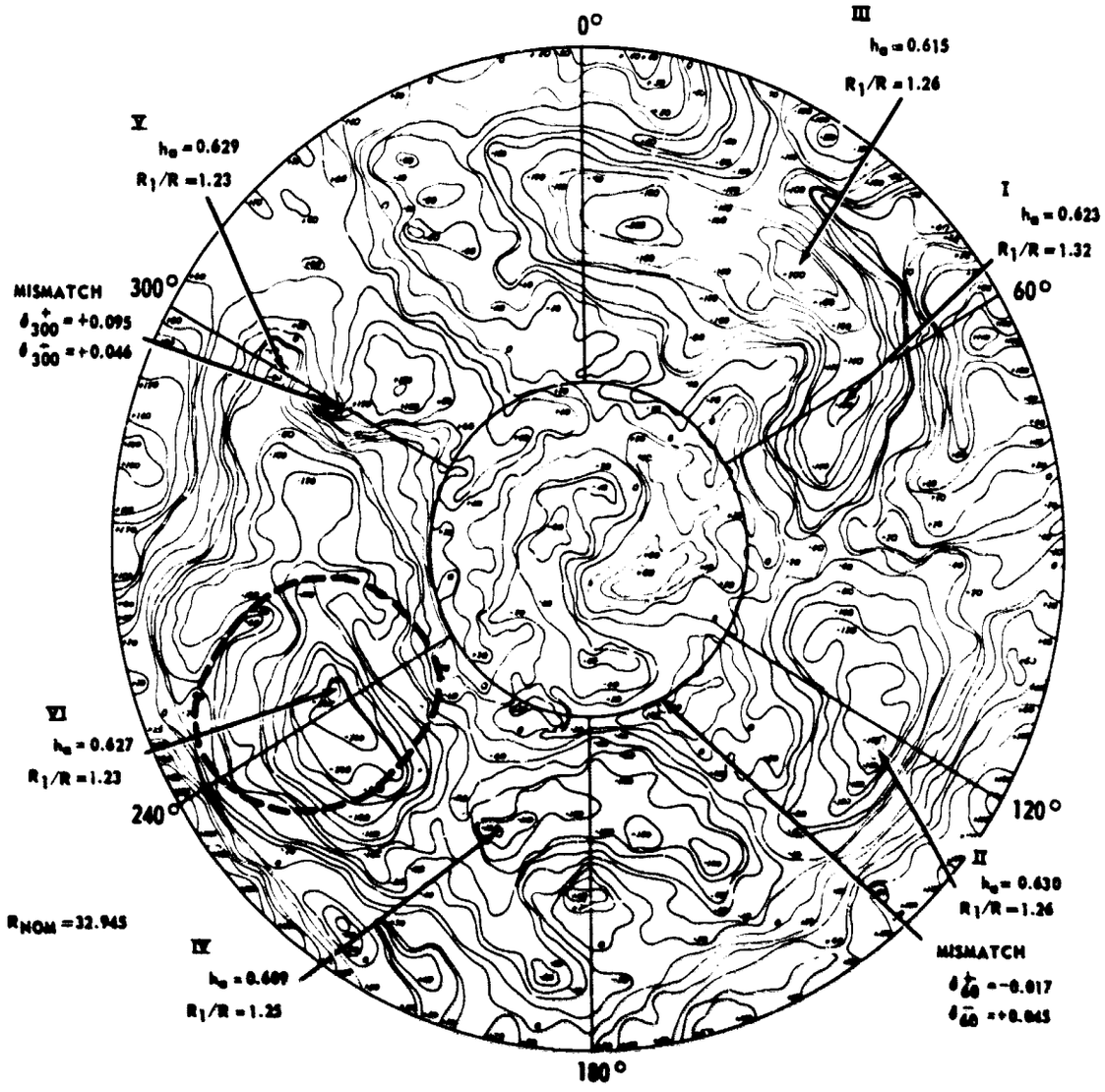

Figure 4b - Model AF-2

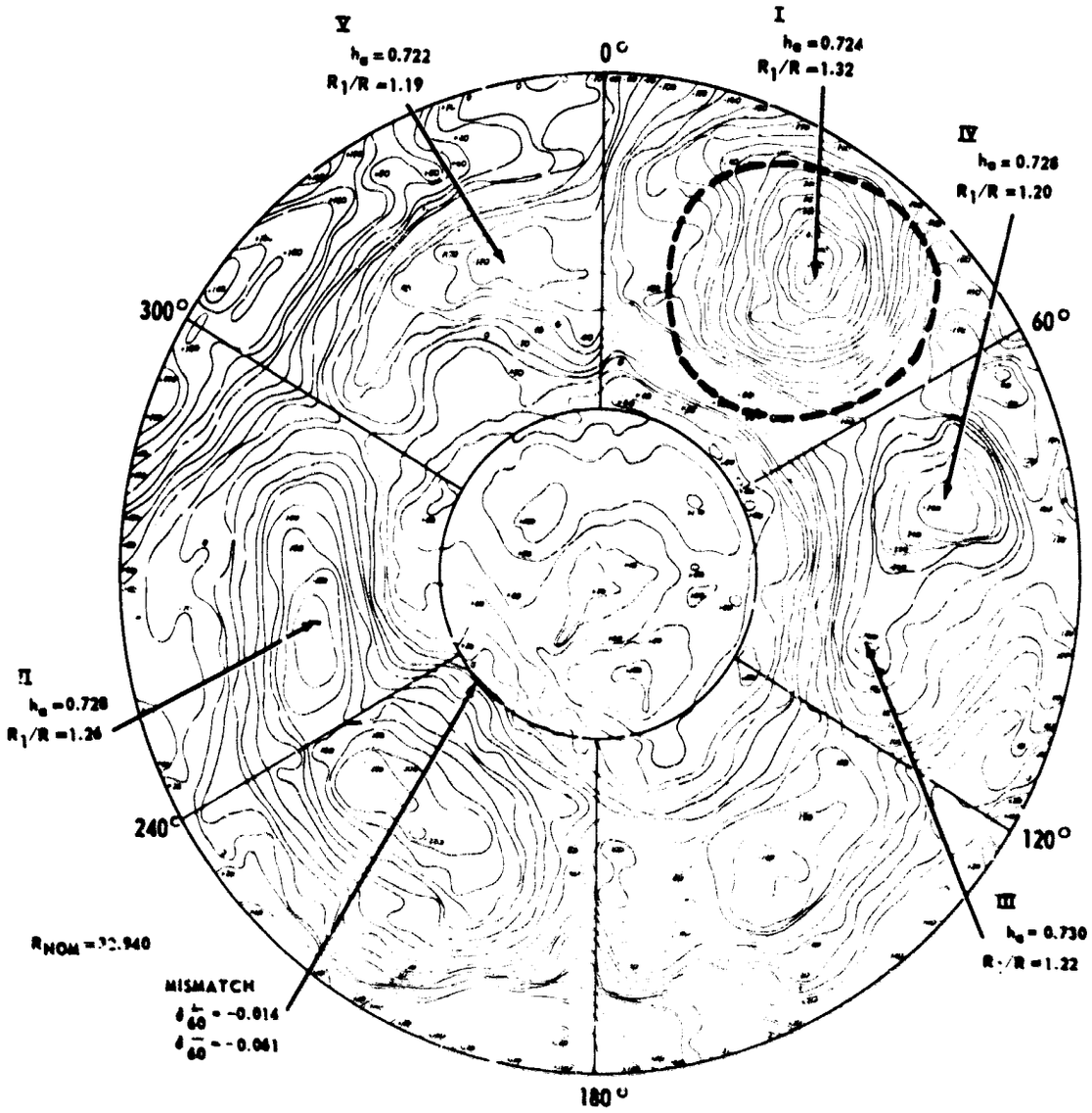

Figure 4c - Model AF-3

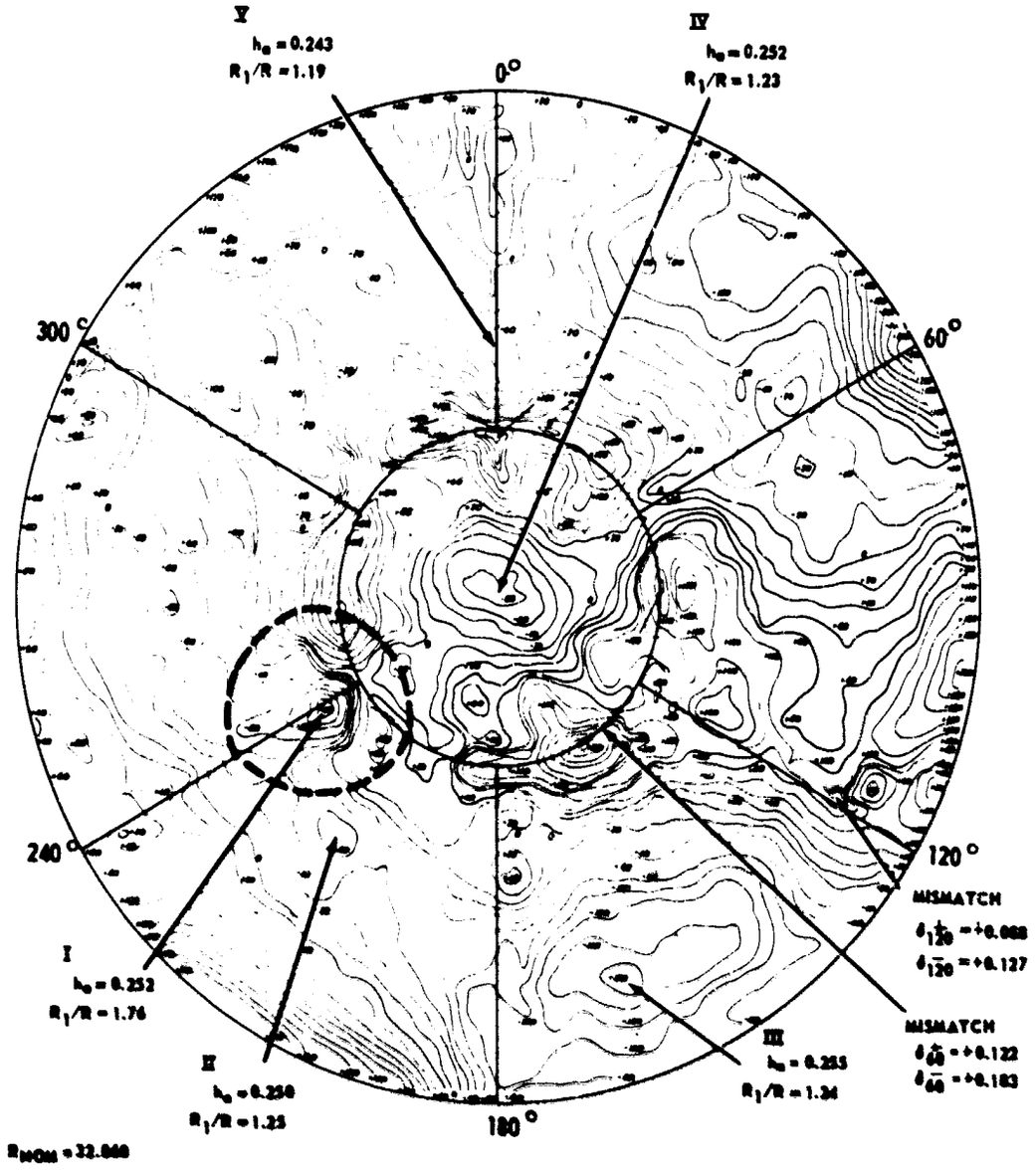

Figure 4d - Model SRS-1

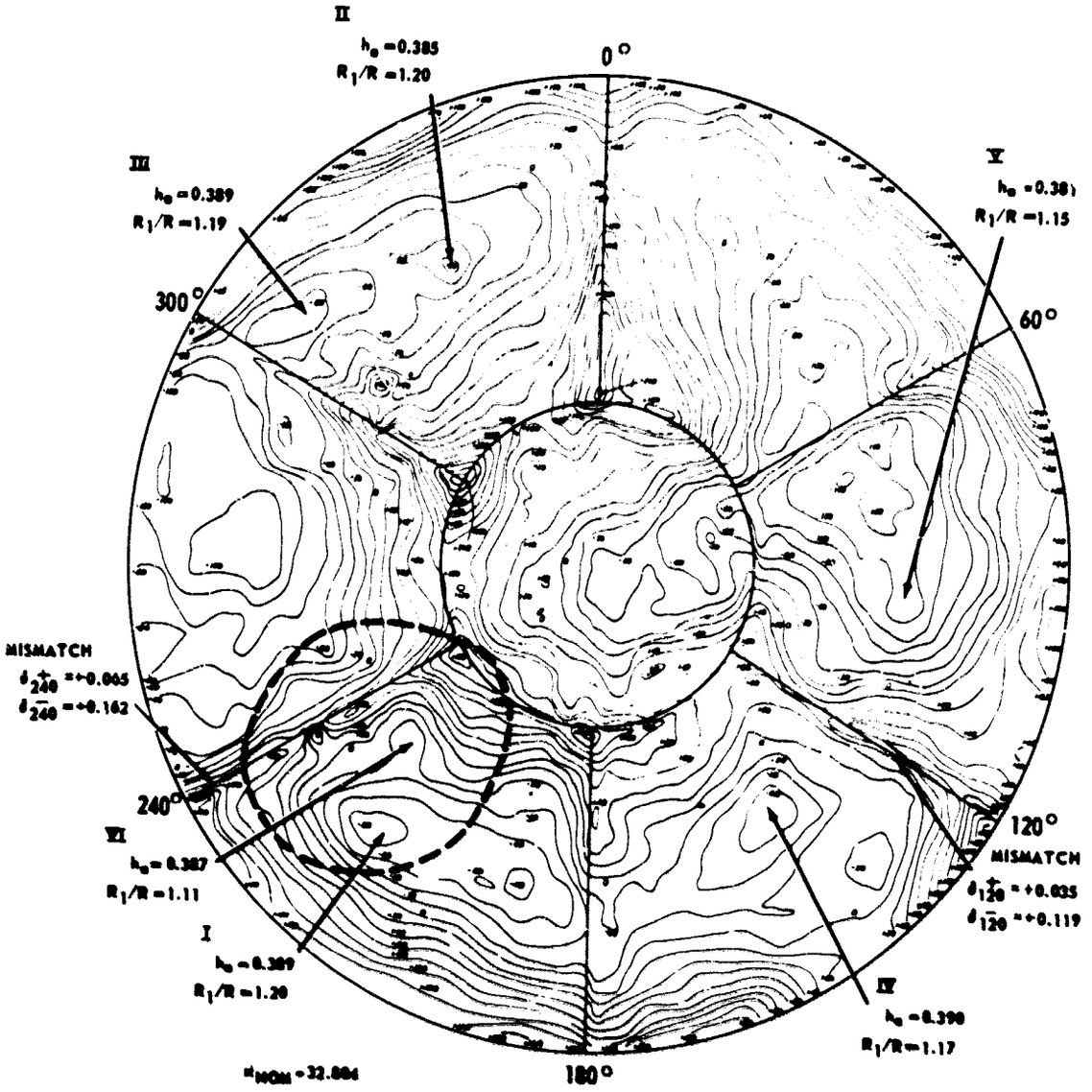

Figure 4e - Model SRS-2

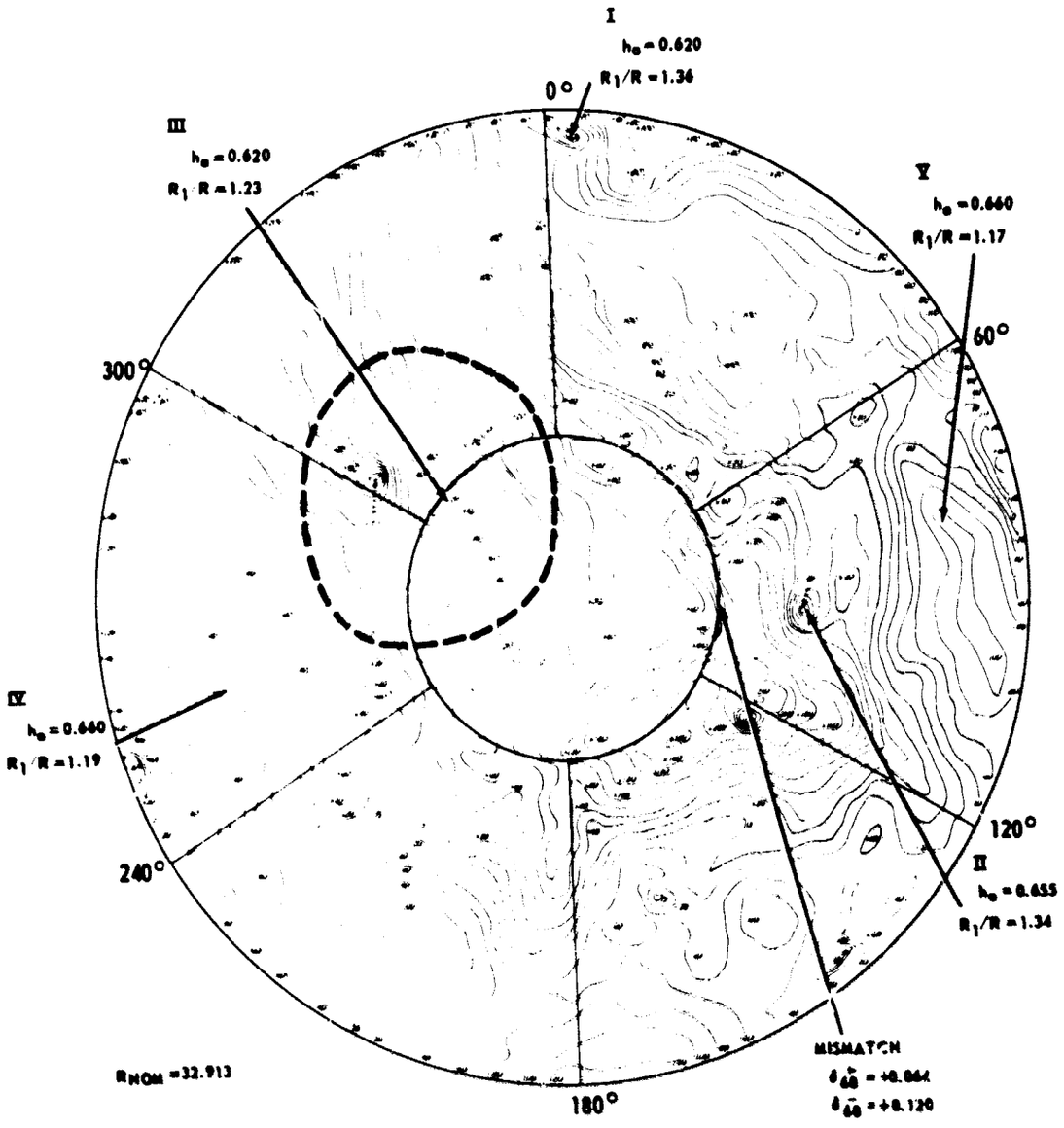

Figure 4f - Model SRS-3

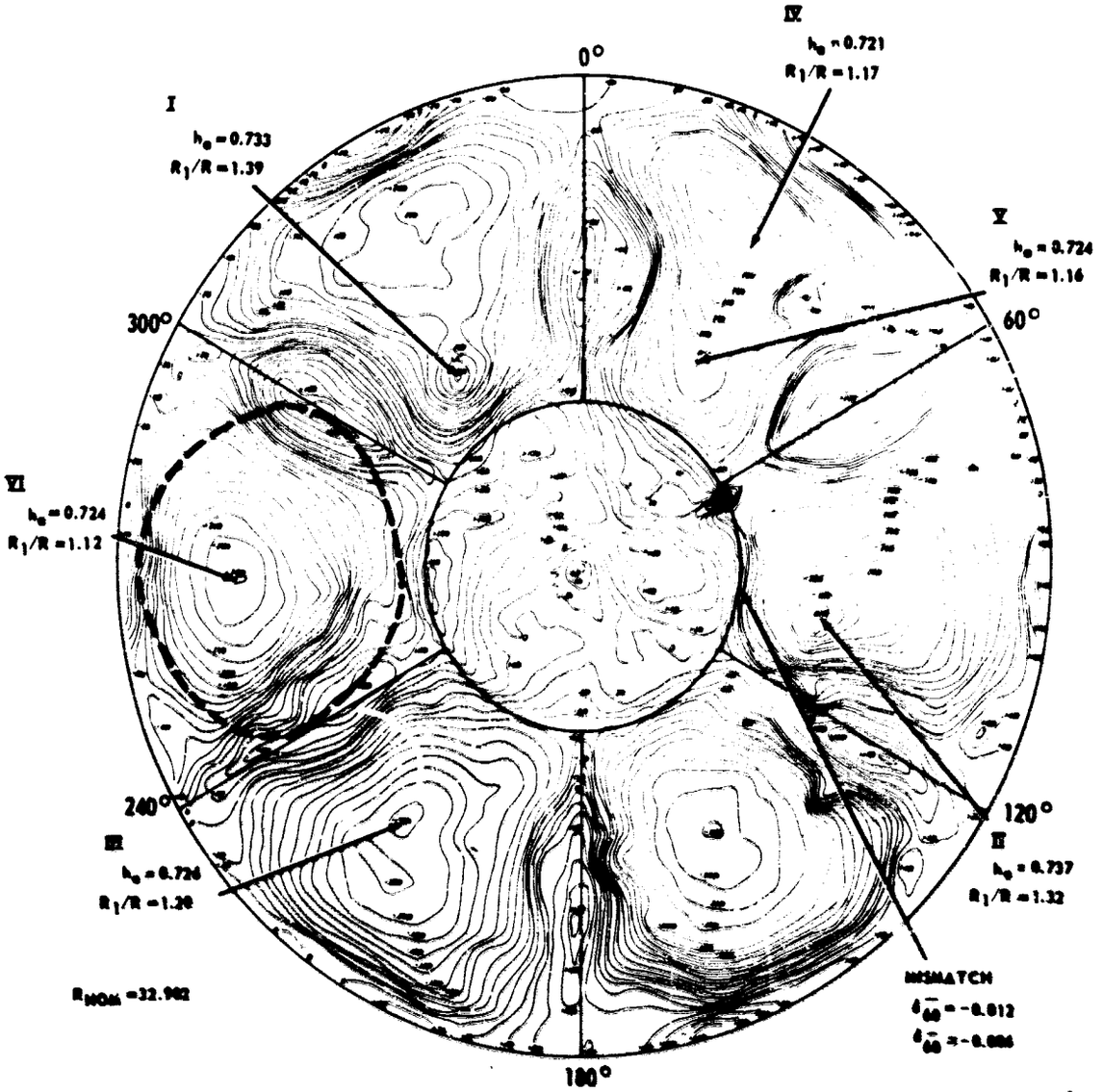

Figure 4g - SRS-4

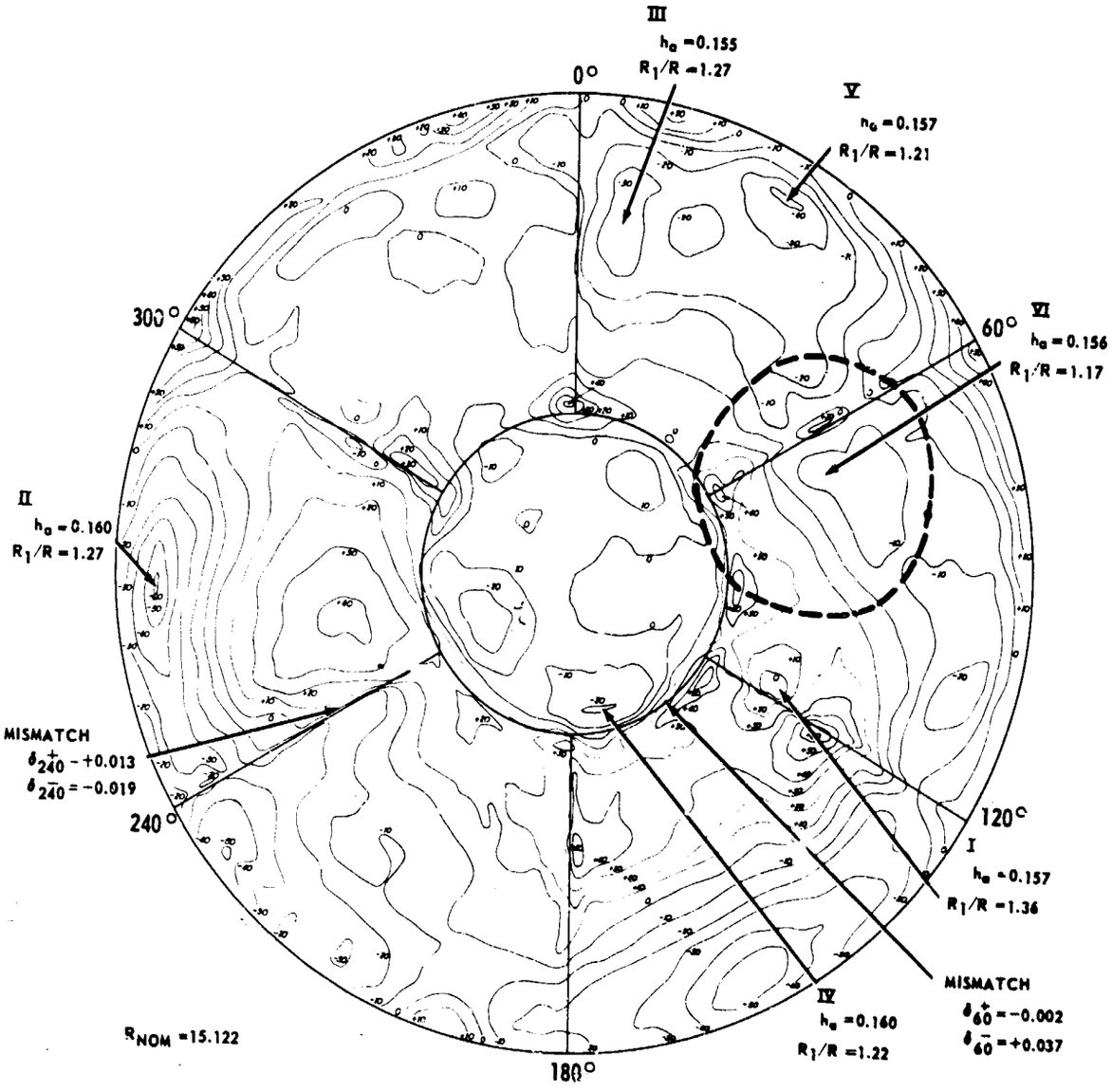

Figure 4h - Model SRS-2A

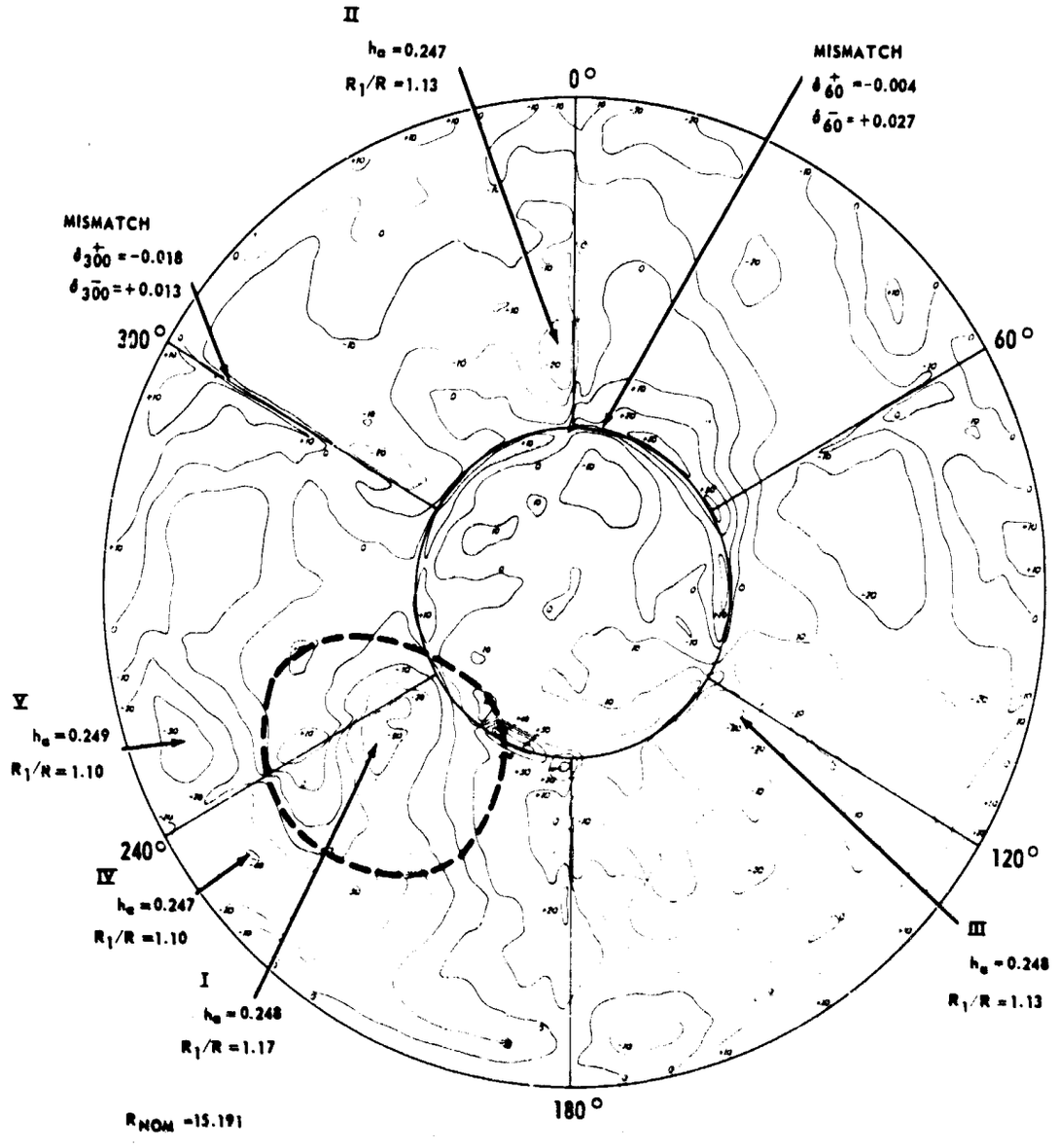

Figure 4i - Model SRS-3A

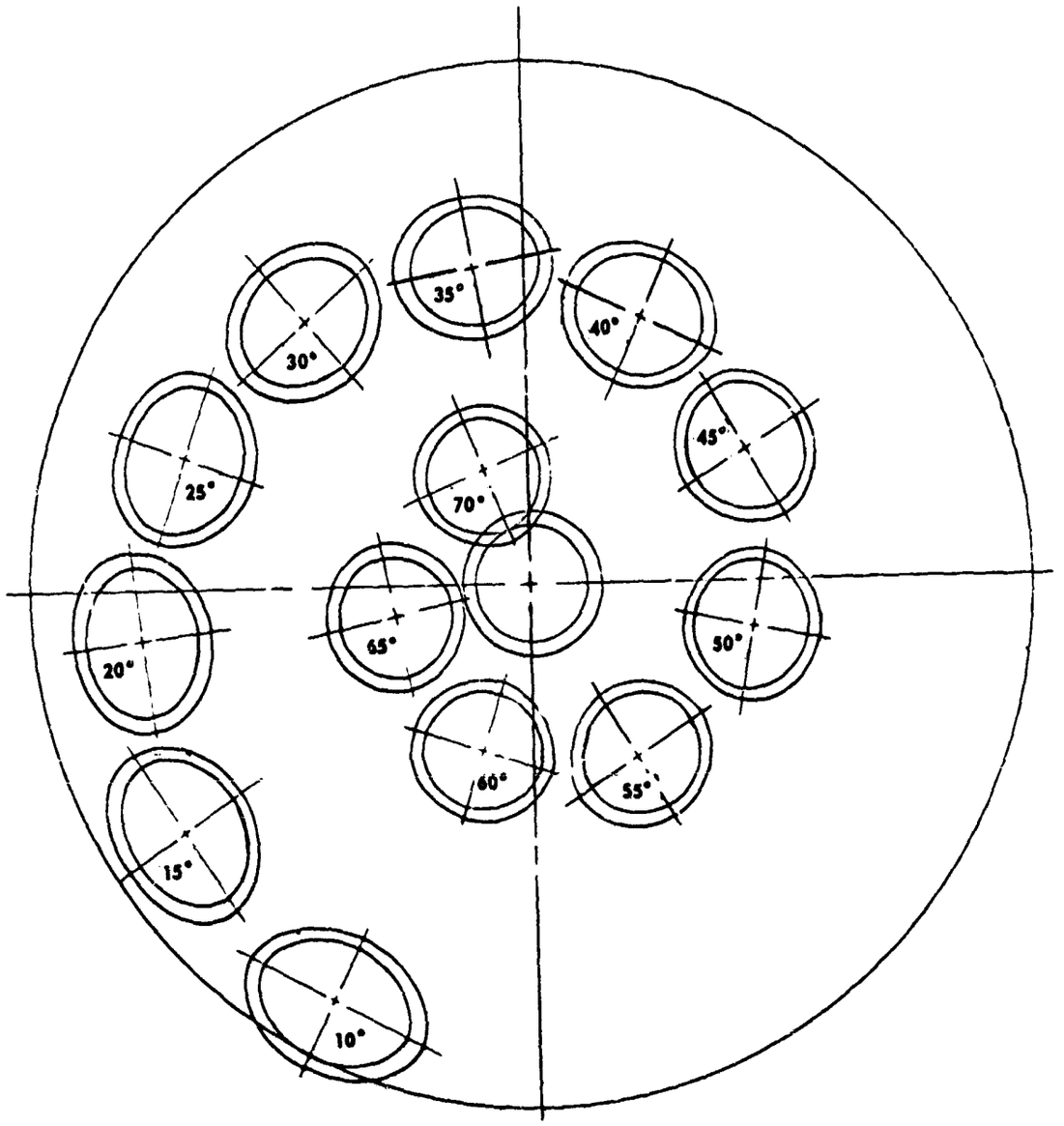

THE SURFACE ENCLOSED BY THE SOLID CIRCLE SHOWN REPRESENTS A HEMISPHERE ROLLED OUT INTO A FLAT SURFACE WHOSE RADIAL SCALE REMAINS CONSTANT.

Figure 5 - Arc Length Scales

Figure 6 - Strain Gage Locations and Strain Sensitivities

The layout shown represents a view looking into the open end of the model except where noted. Both inside and outside surfaces are instrumented for each position indicated. All inside gages have numbers begining with 200 and all outside with numbers begining with 100 (only the outside gages are indicated on these diagrams). All circumferential gage numbers end with an even number and all meridional gages with an odd number. All gages oriented 45 deg from these directions have numbers ending with the letter A. The strain sensitivity for each gage is given in parenthesis adjacent to the gage in μin./in./psi. The figure on the left is the sensitivity for the outside and the right for the inside. * indicates gage for which pressure strain plots are shown on Figure 8. The area of failure is indicated by broken line.

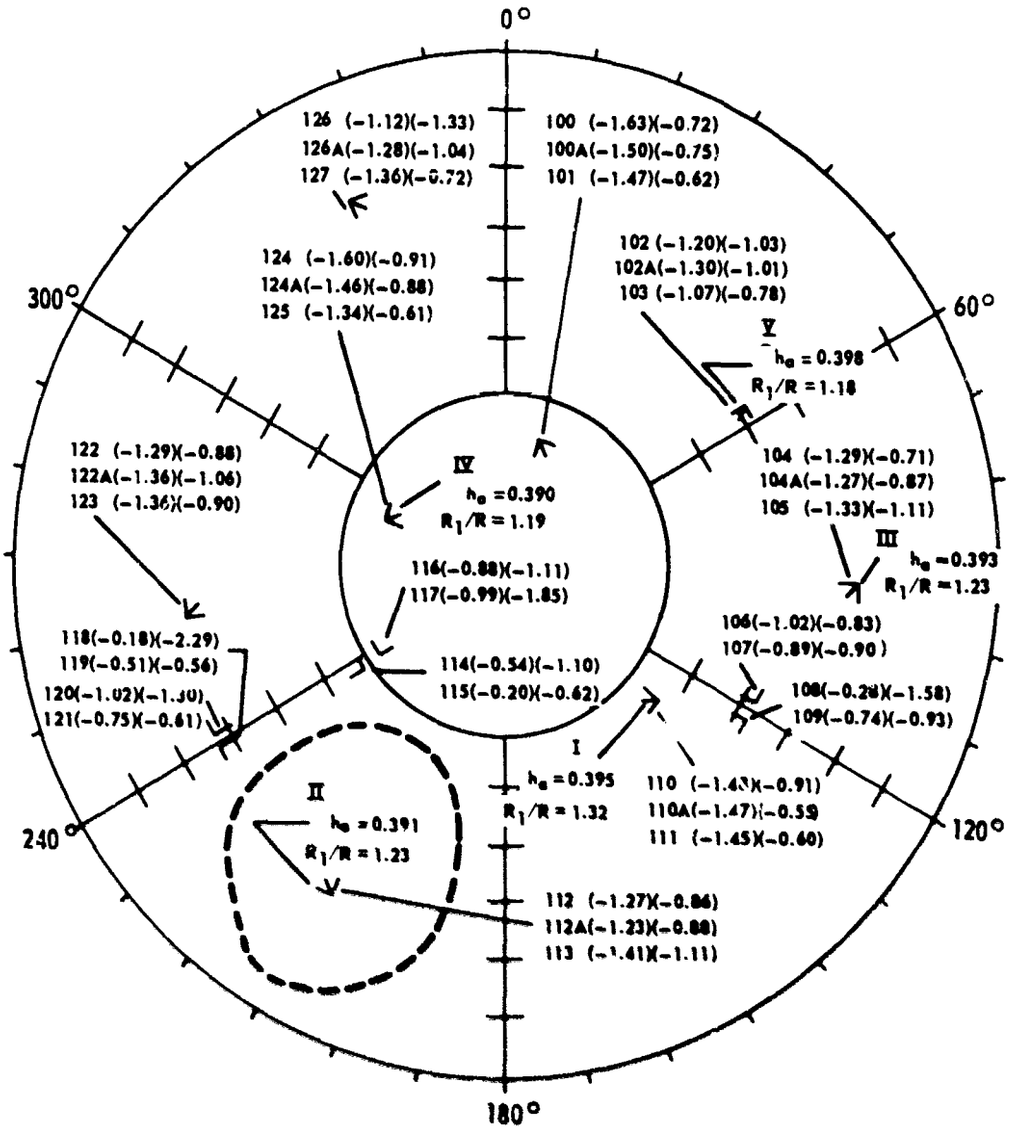

Figure 6a - Model AF-1

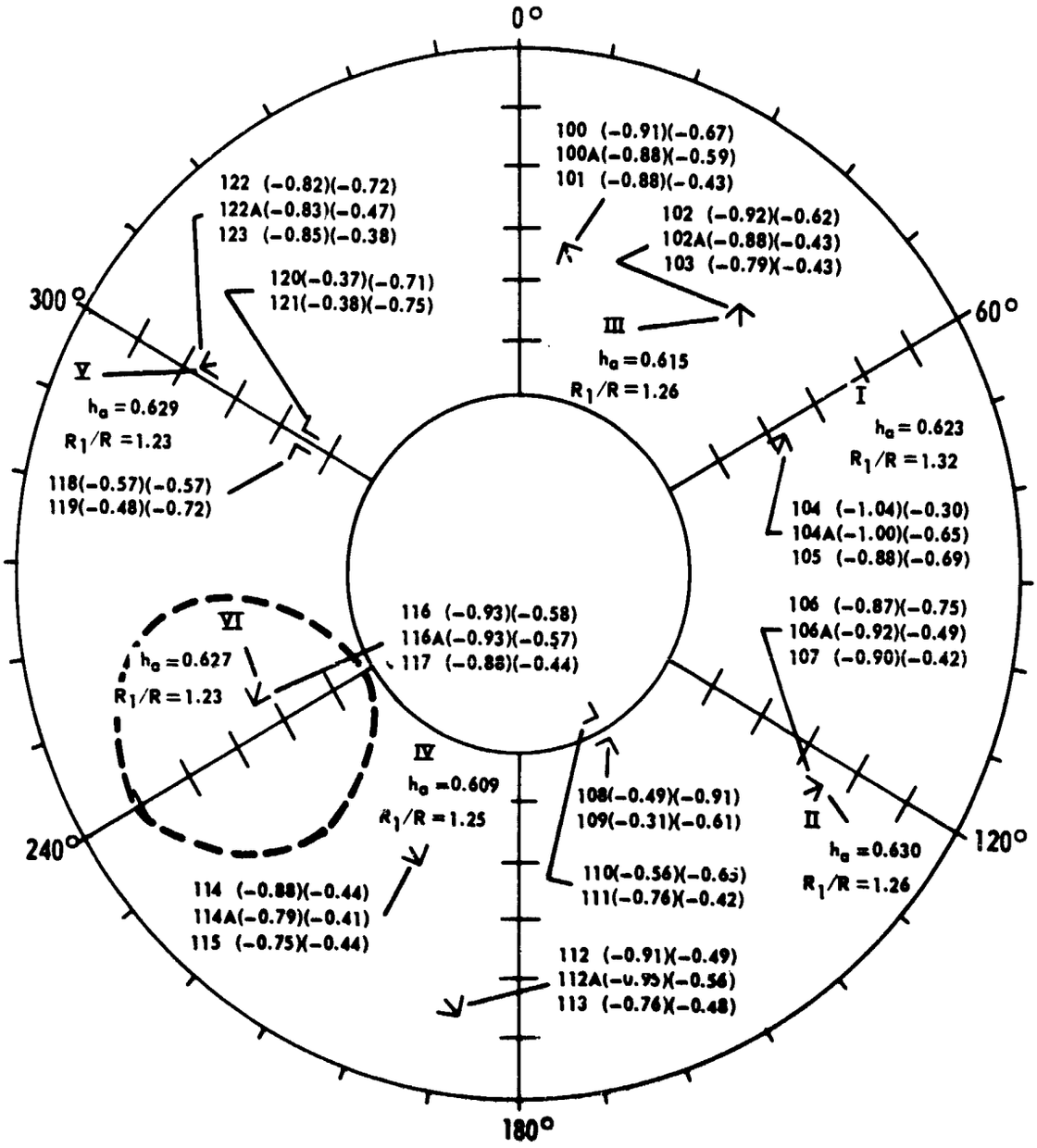

Figure 6b - Model AF-2

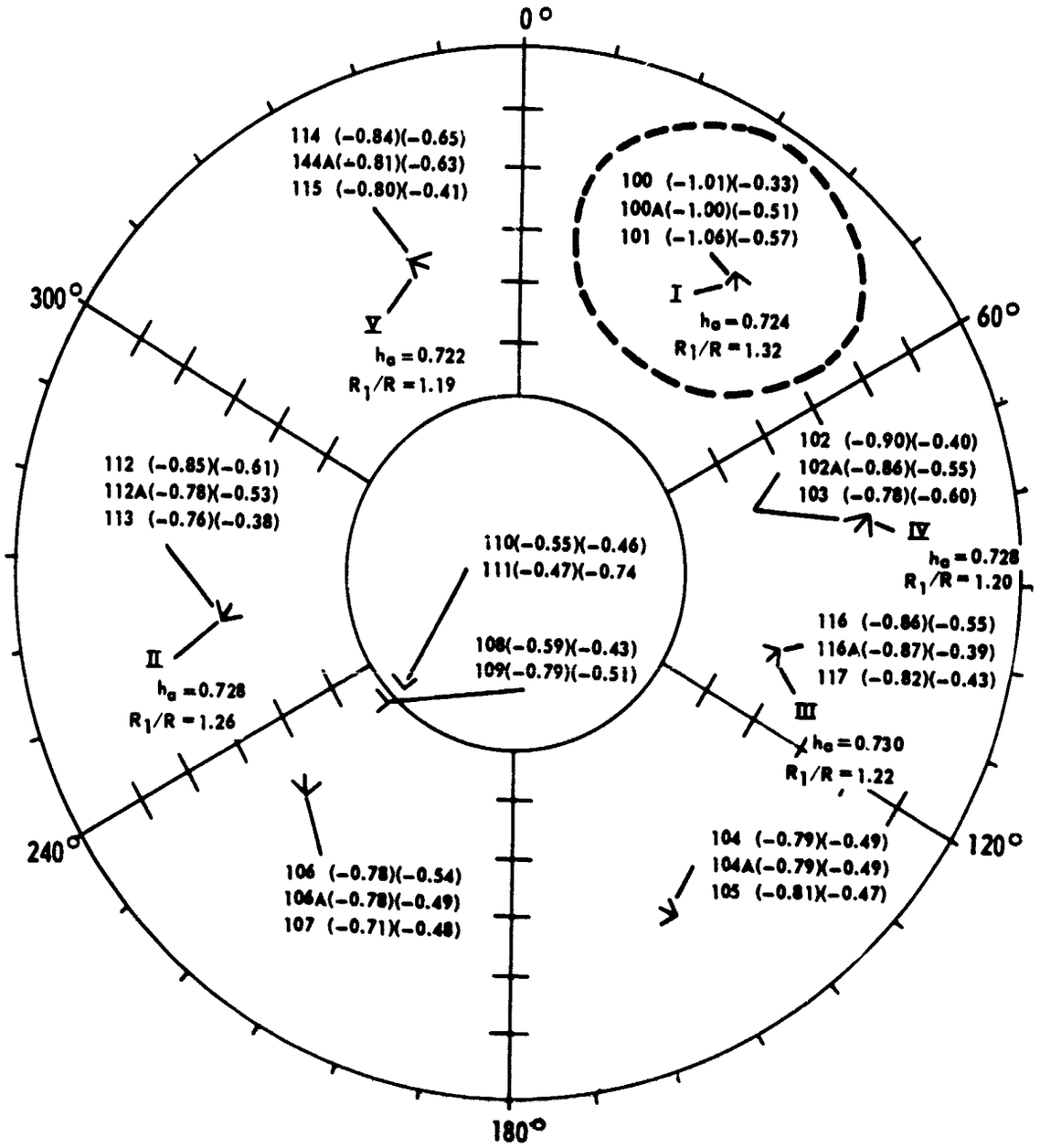

Figure 6c - Model AF-3

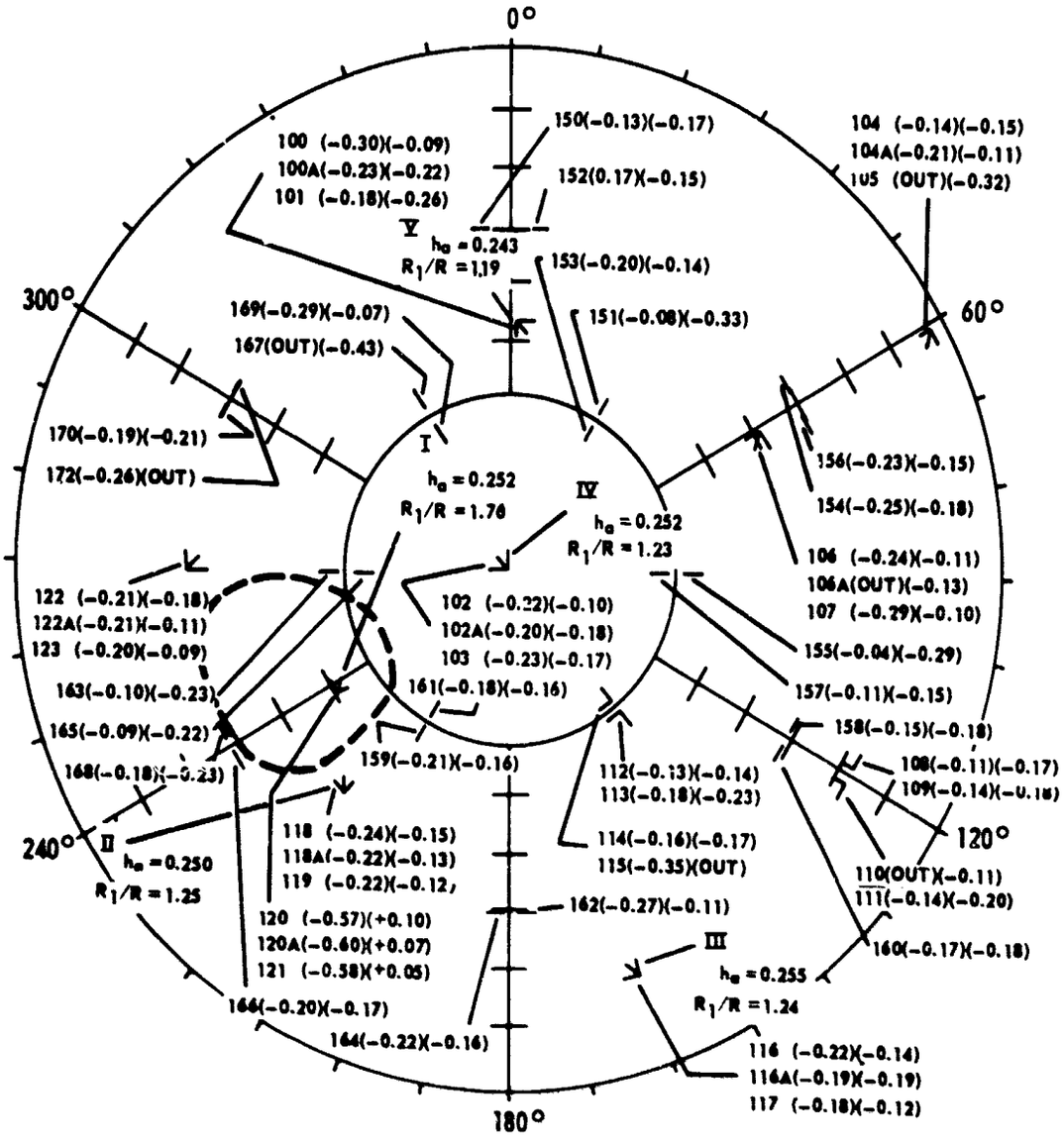

Figure 6d - Model SRS-1

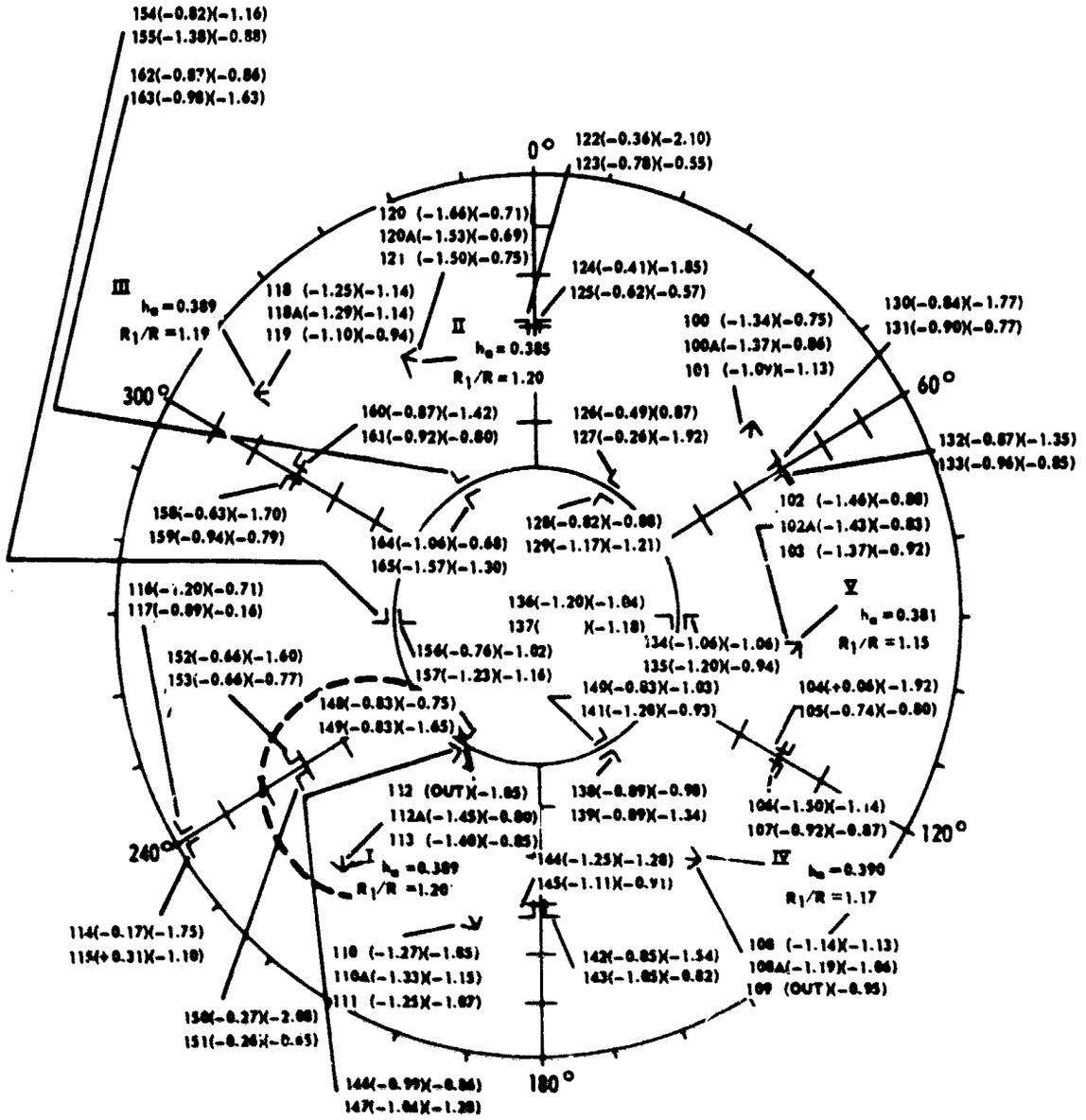

Figure 6e - Model SRS-2

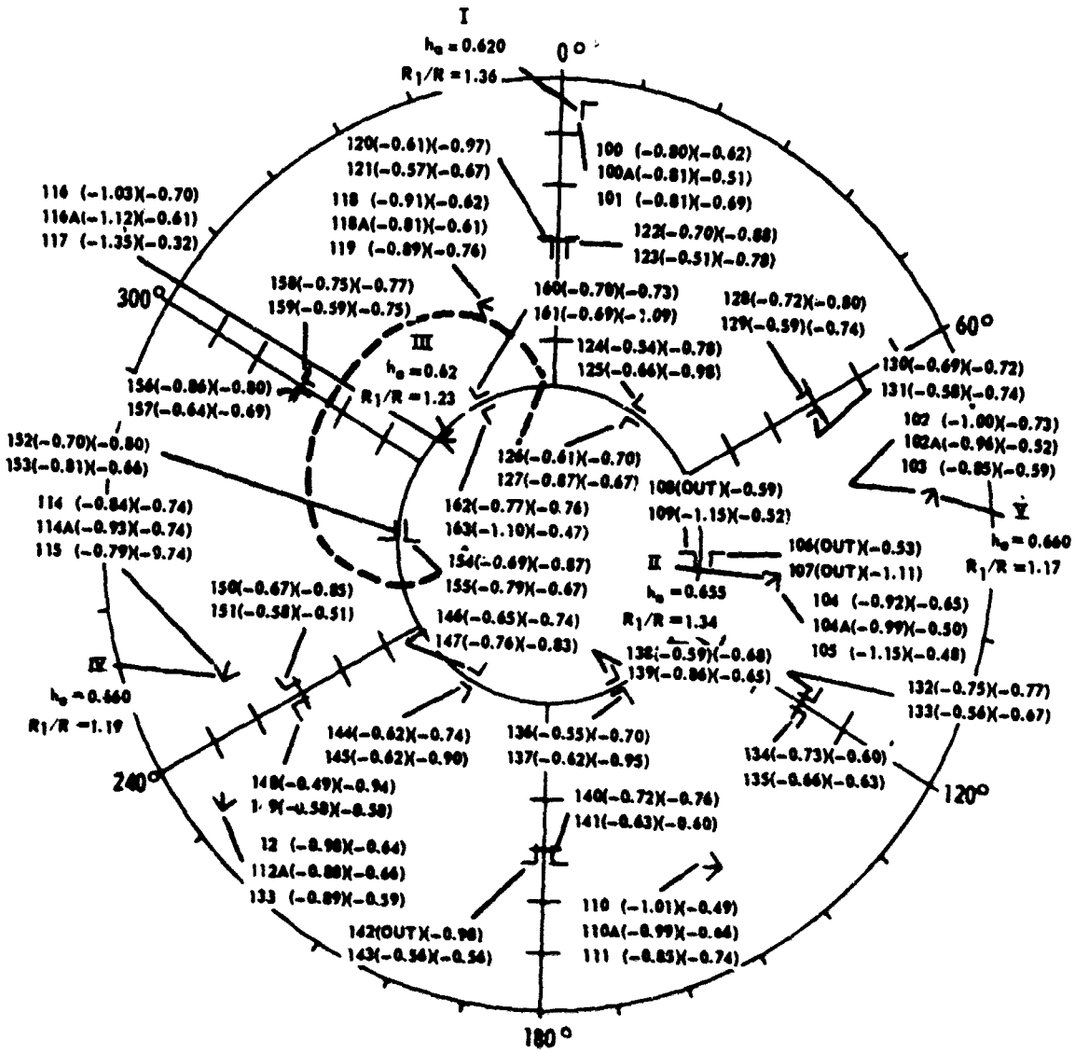

Notes:
1. View is looking down on the outside of the model.
2. Strain sensitivities for gages 100 through 134 are from the third pressure run only with recorded data modified to compensate for erratic gage behavior.

Figure 6f - Model SRS-3

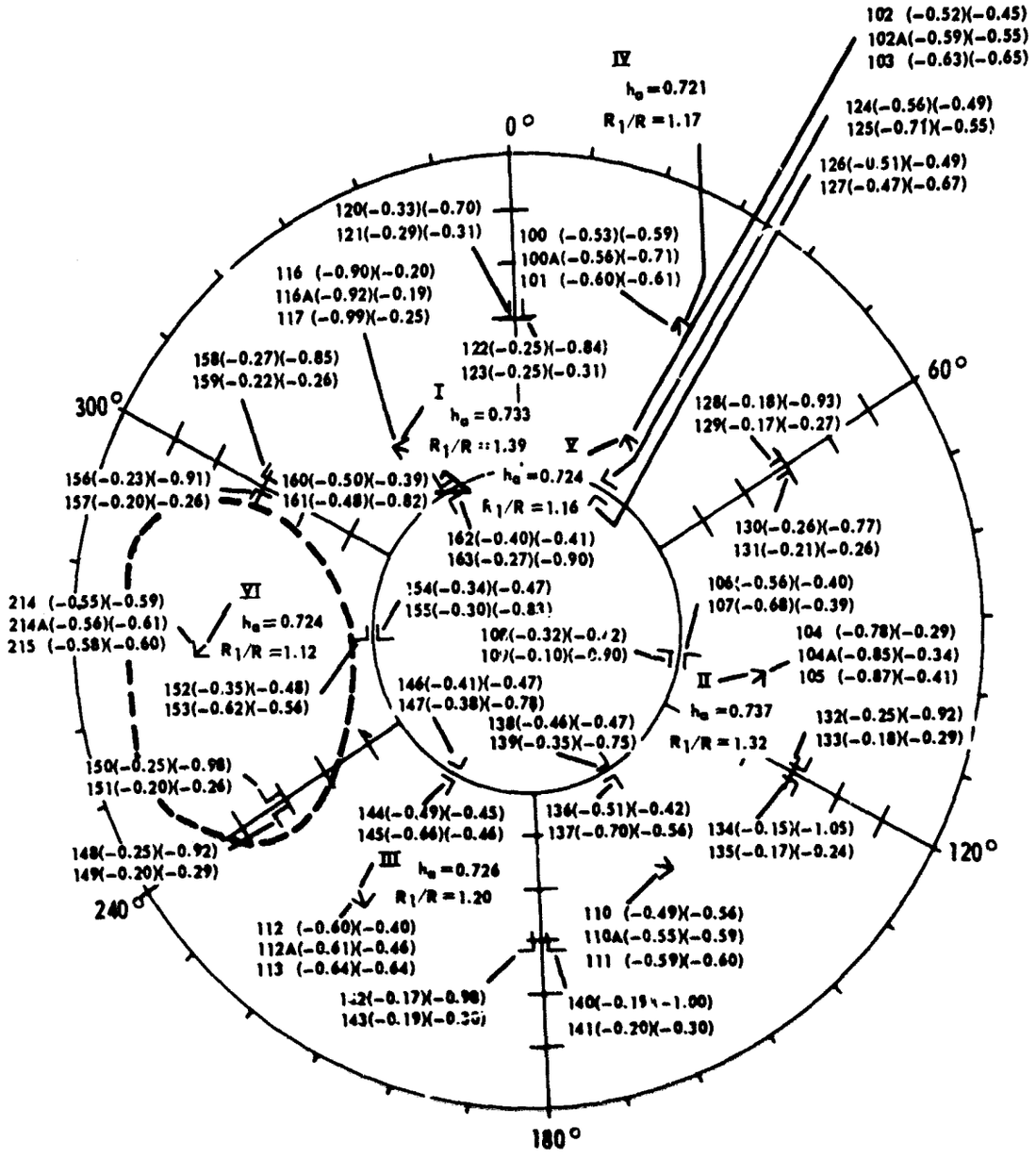

Figure 6g - Model SRS-4

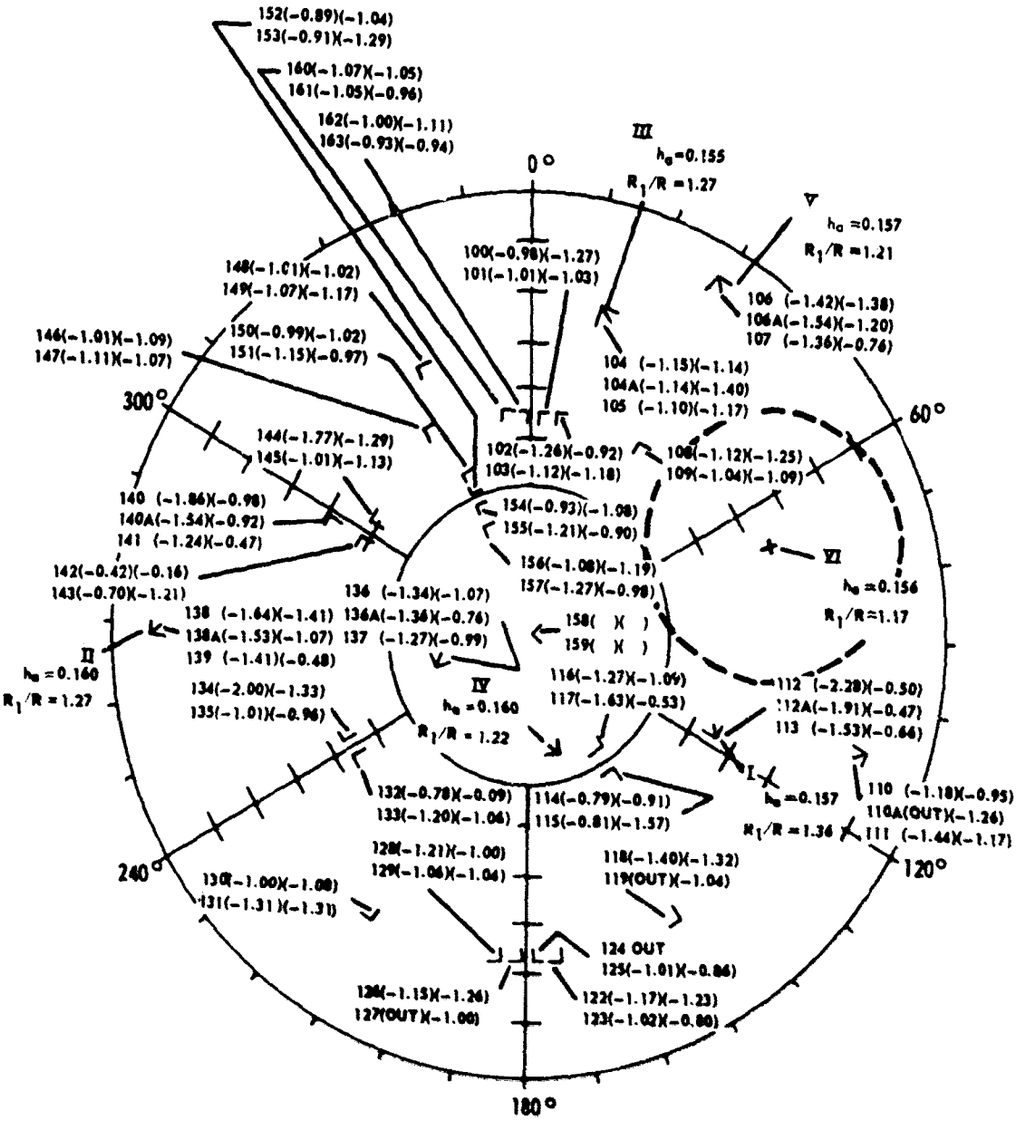

Figure 6h - Model SRS-2A

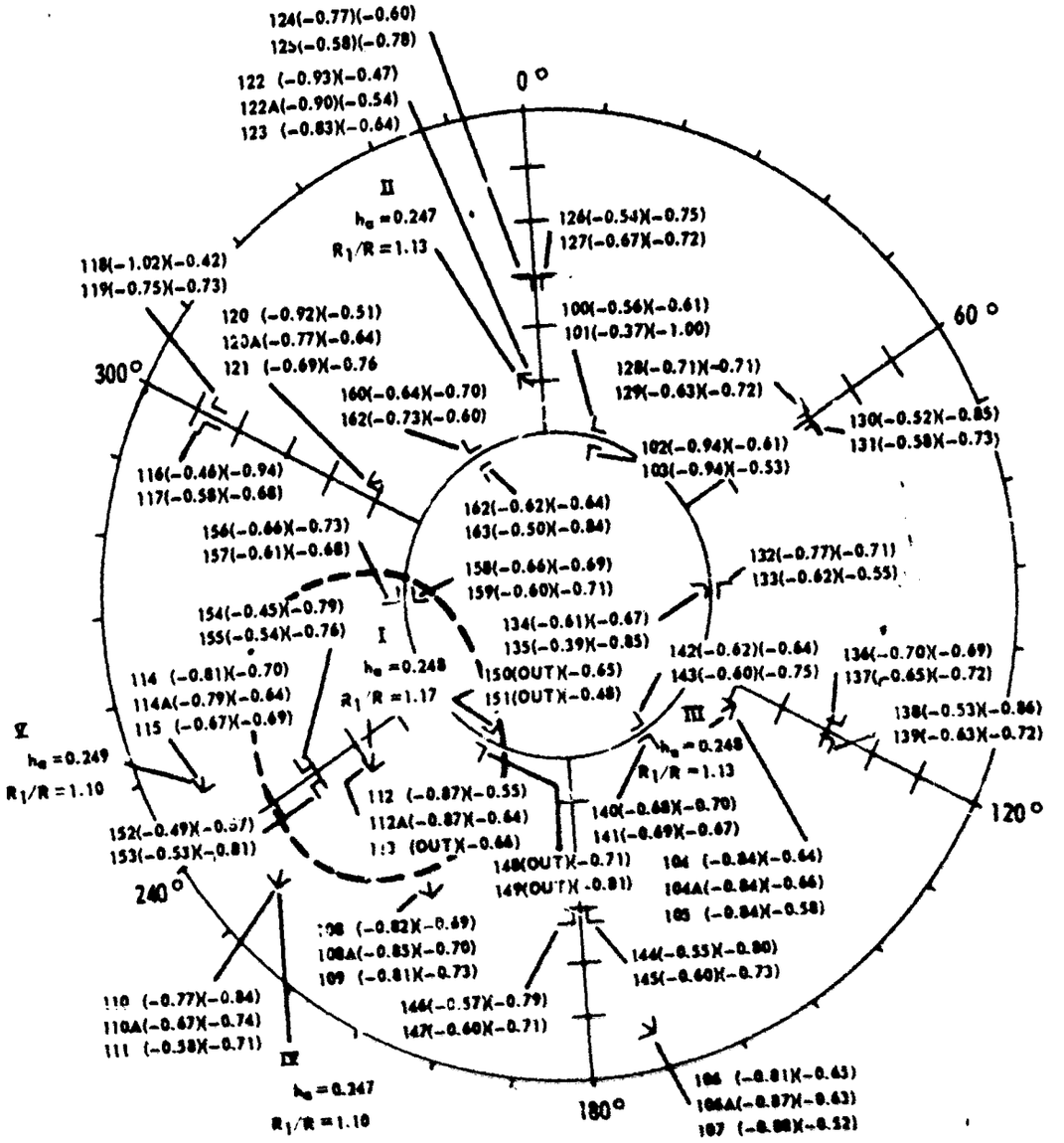

Figure 6i - Model SRS-3A

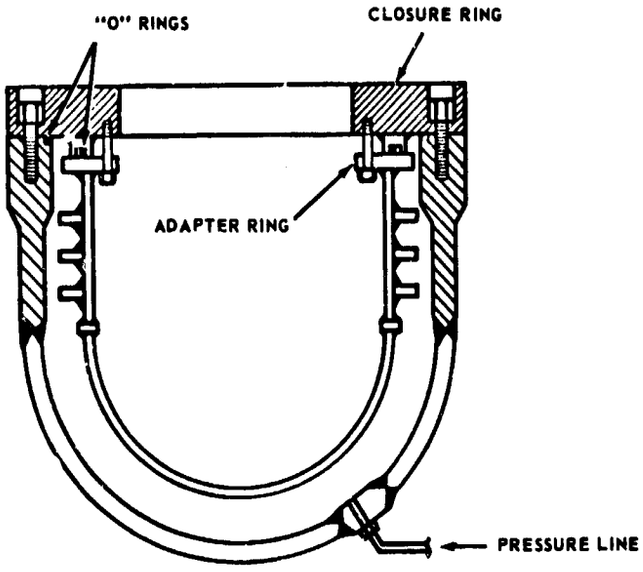

Figure 7a - 6-Foot Head Testing Tank

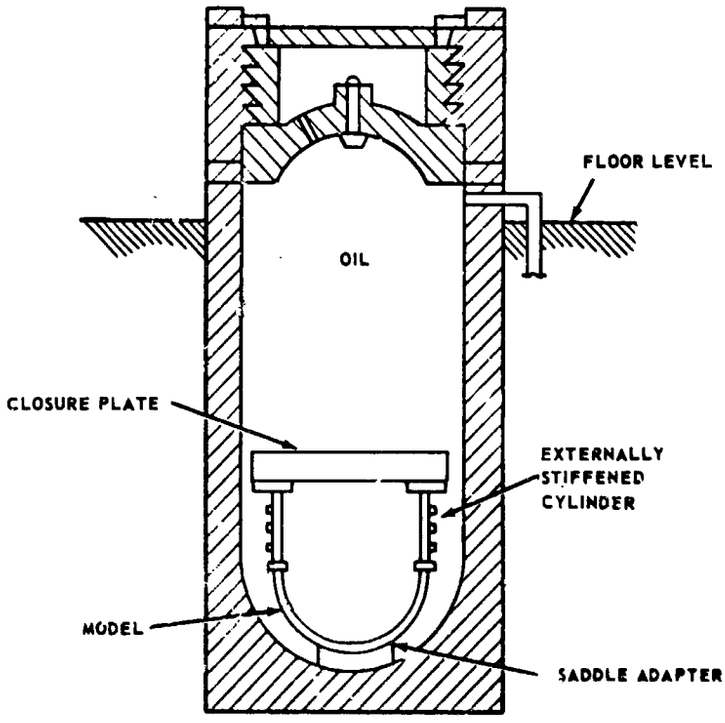

Figure 7b - 4-Foot Testing Tank

Figure 7 - Test Setup

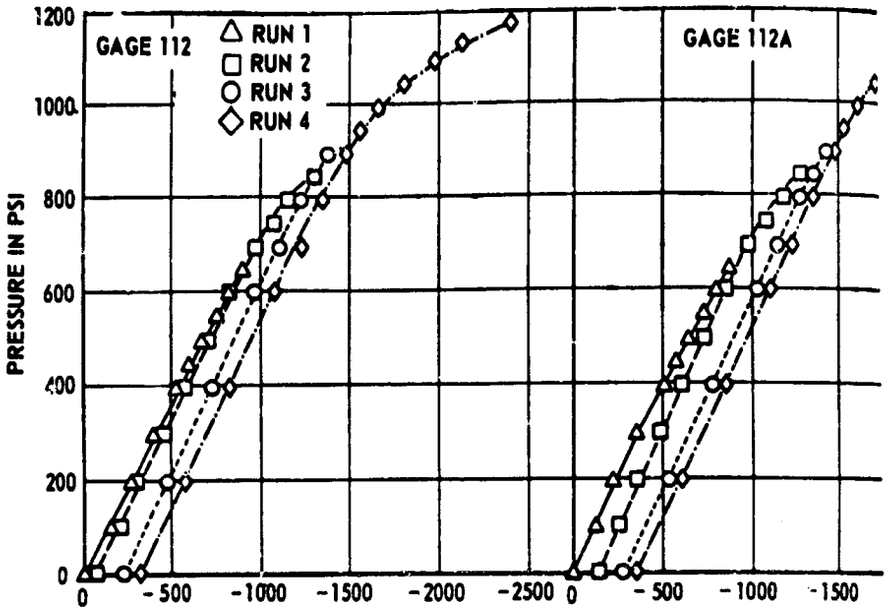
GAGE 112
RUN 1
RUN 2
RUN 3
RUN 4
GAGE 112A
PRESSURE IN PSI
1200
1000
800
600
400
200
0
0
-500
-1000
-1500
-2000
-2500
0
-500
-1000
-1500

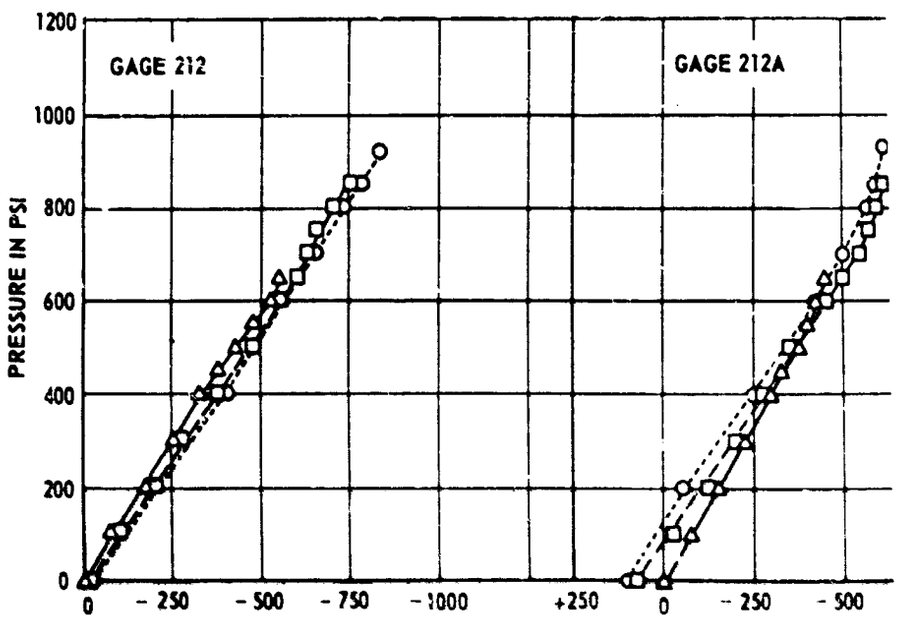
GAGE 212
GAGE 212A
PRESSURE IN PSI
1200
1000
800
600
400
200
0
0
-250
-500
-750
-1000
+250
0
-250
-500

Figure 8 - Typical Pressure-Strain Plots

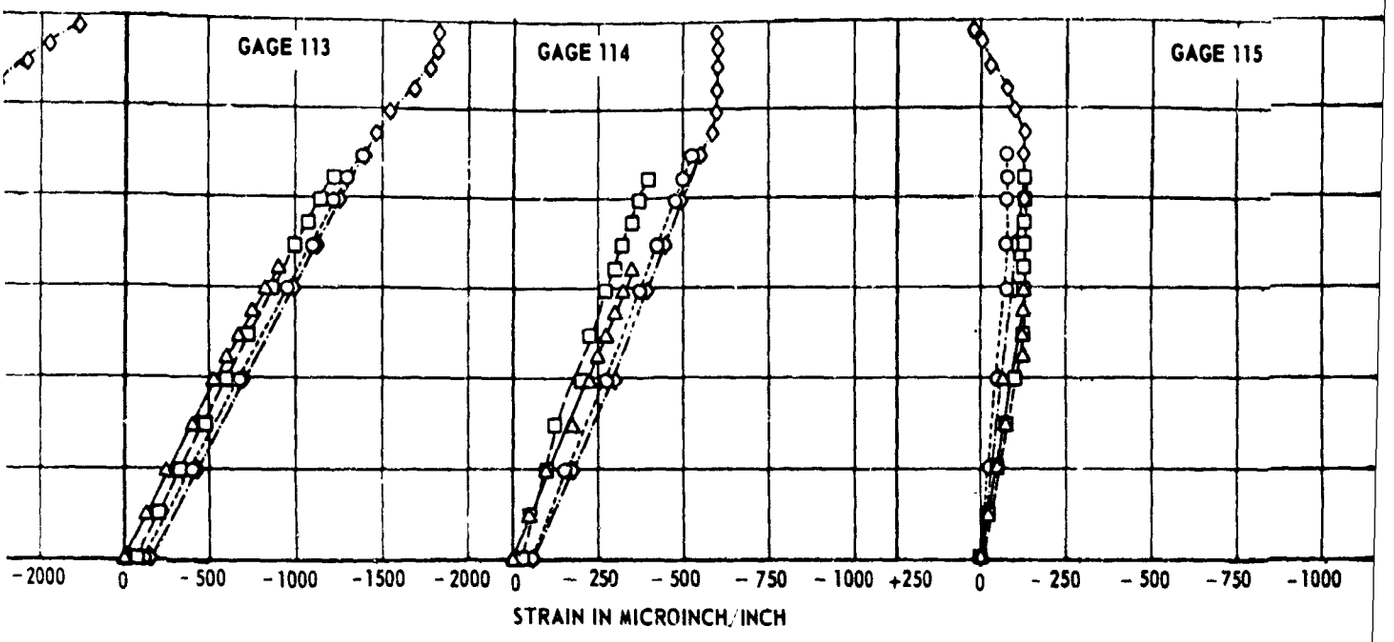

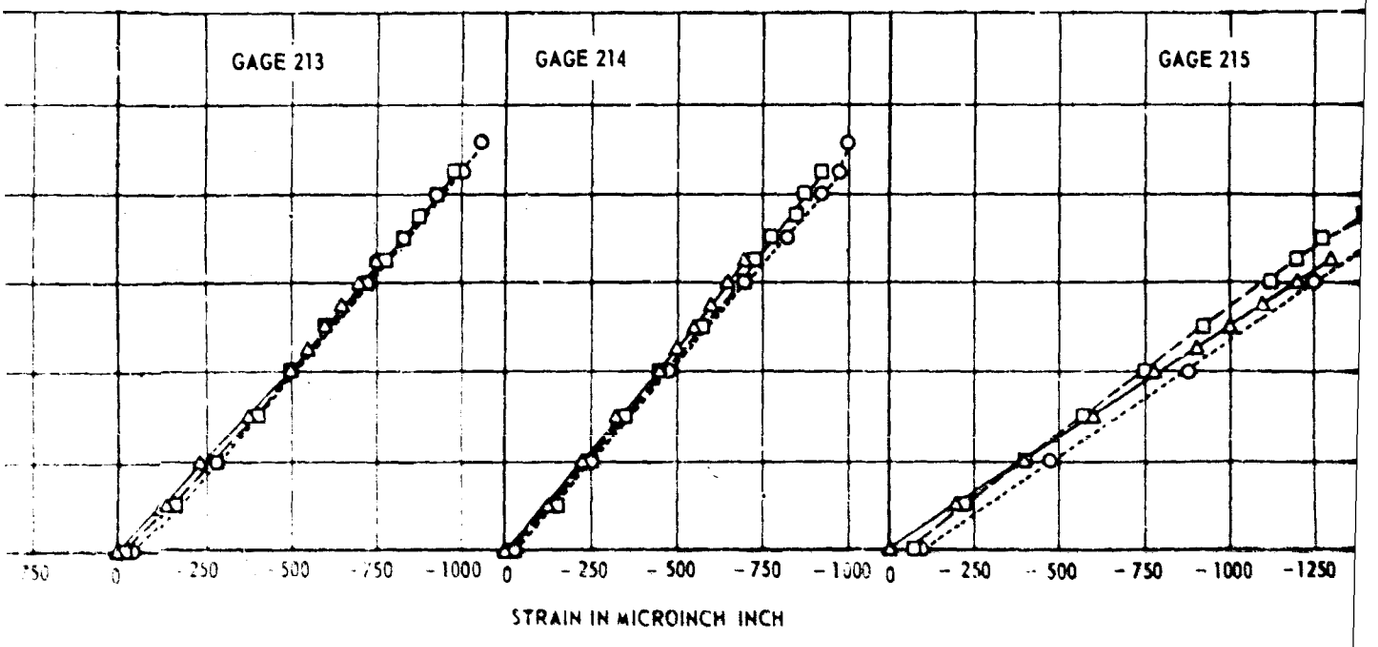

Figure 8a - Model AF-1

n Plots

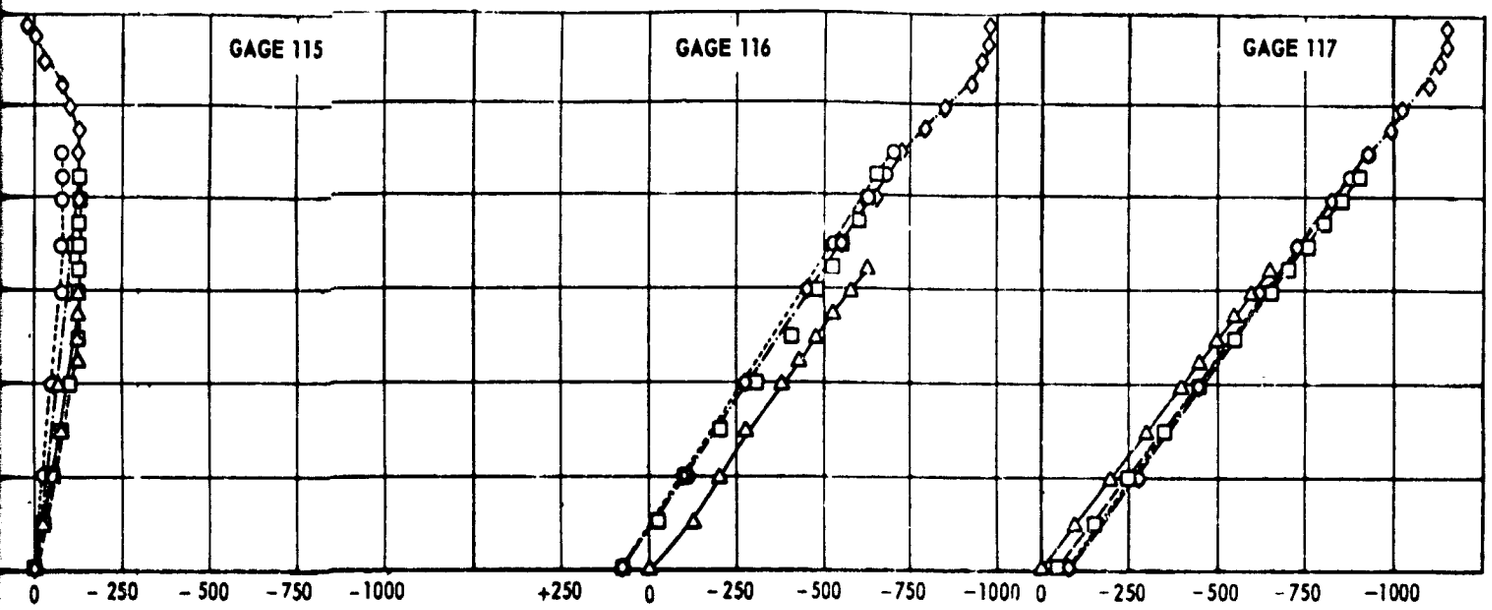
GAGE 115
GAGE 116
GAGE 117
0
- 250
- 500
- 750
-1000
+250
0
- 250
- 500
- 750
-1000
0
- 250
- 500
- 750
-1000

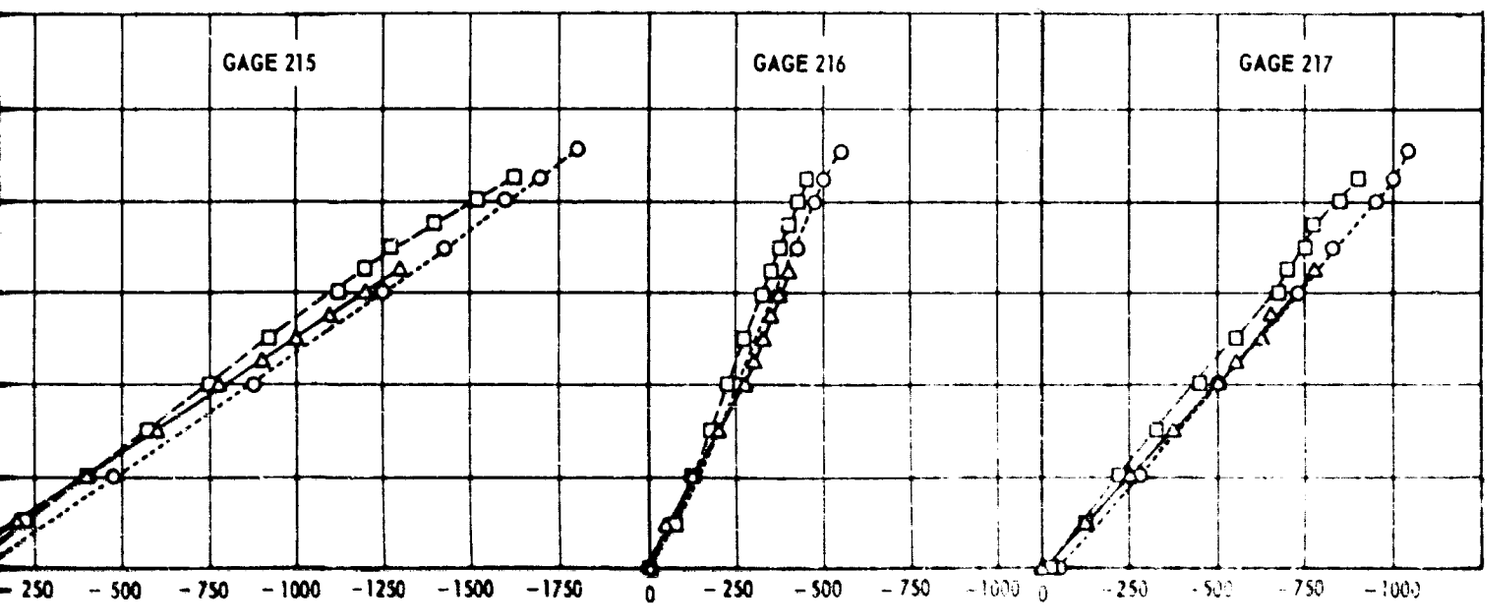
GAGE 215
GAGE 216
GAGE 217
- 250
- 500
- 750
- 1000
-1250
-1500
-1750
0
- 250
- 500
- 750
-1000
0
- 250
- 500
- 750
-1000

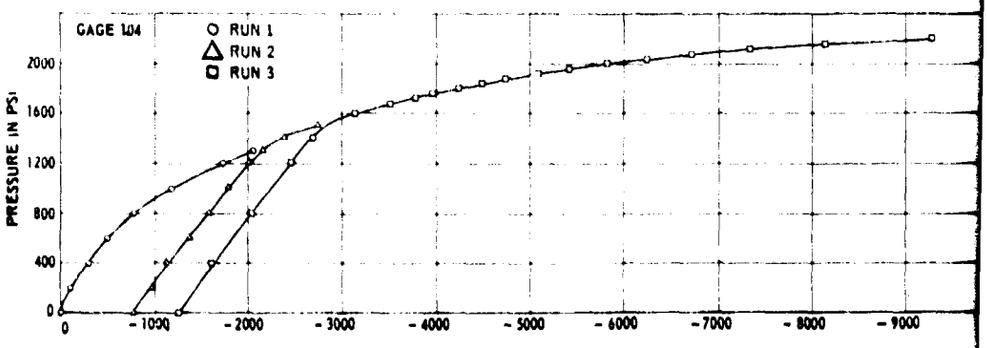
GAGE 104
RUN 1
RUN 2
RUN 3
PRESSURE IN PSI
2000
1600
1200
800
400
0
0
-1000
-2000
-3000
-4000
-5000
-6000
-7000
-8000
-9000

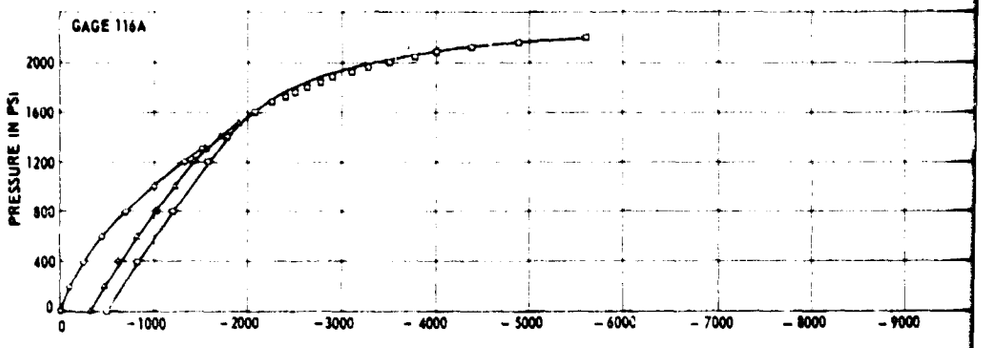
GAGE 116A
PRESSURE IN PSI
2000
1600
1200
800
400
0
0
-1000
-2000
-3000
-4000
-5000
-6000
-7000
-8000
-9000

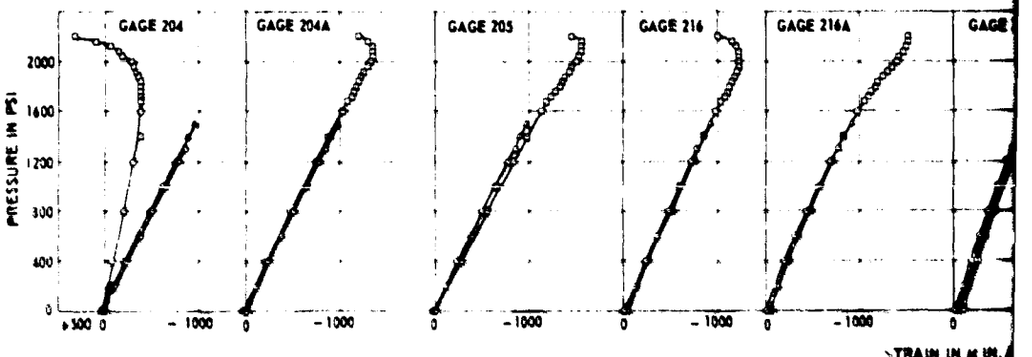
GAGE 204
GAGE 204A
GAGE 205
GAGE 216
GAGE 216A
PRESSURE IN PSI
2000
1600
1200
800
400
0
+500
0
-1000
STRAIN IN

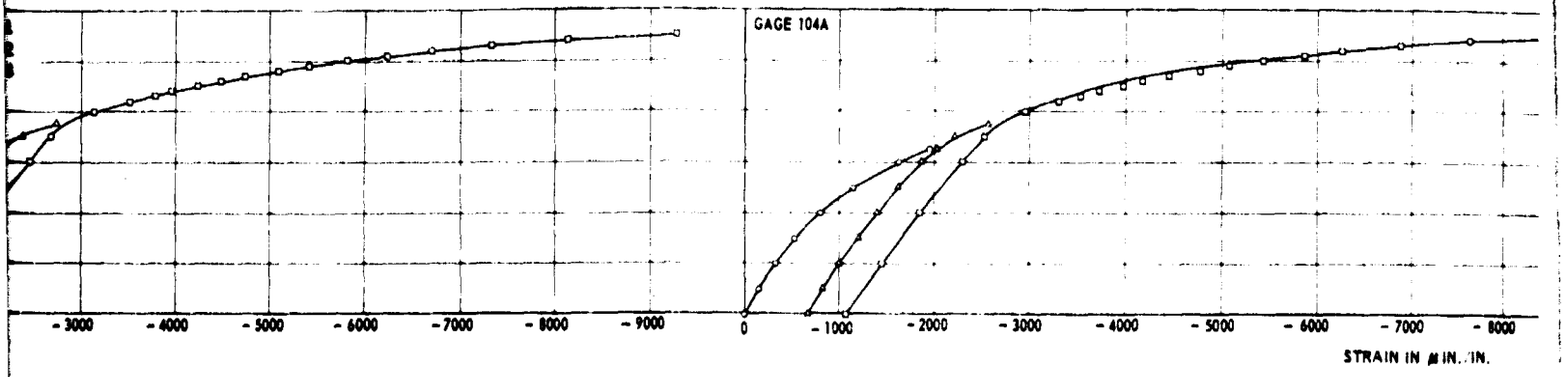

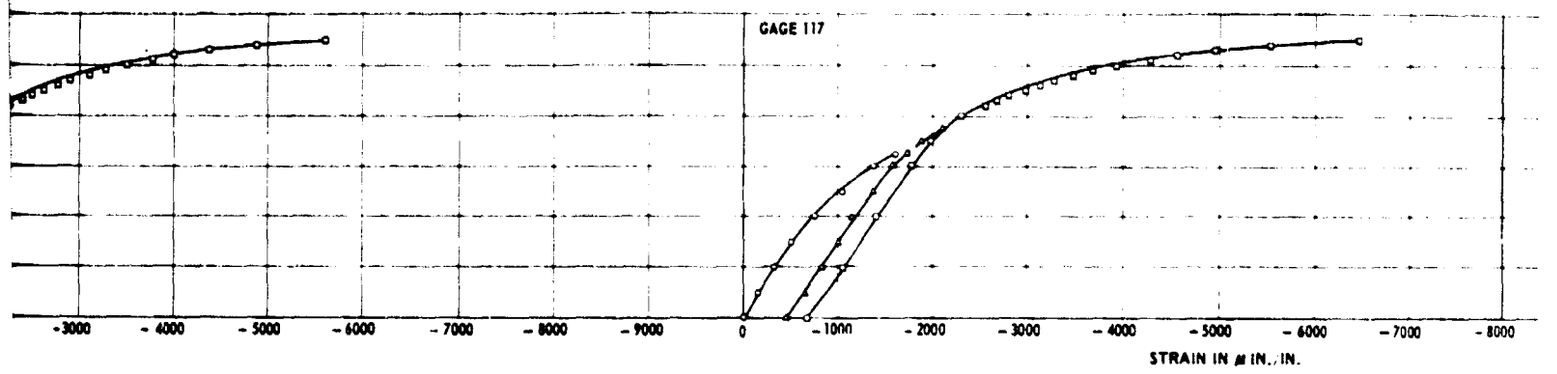

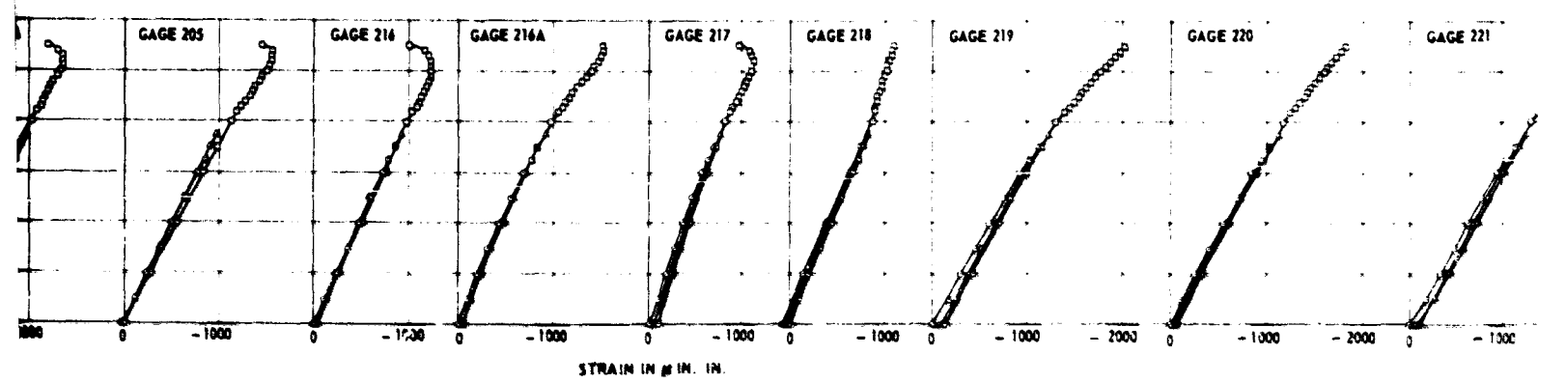

Figure 8b - Model

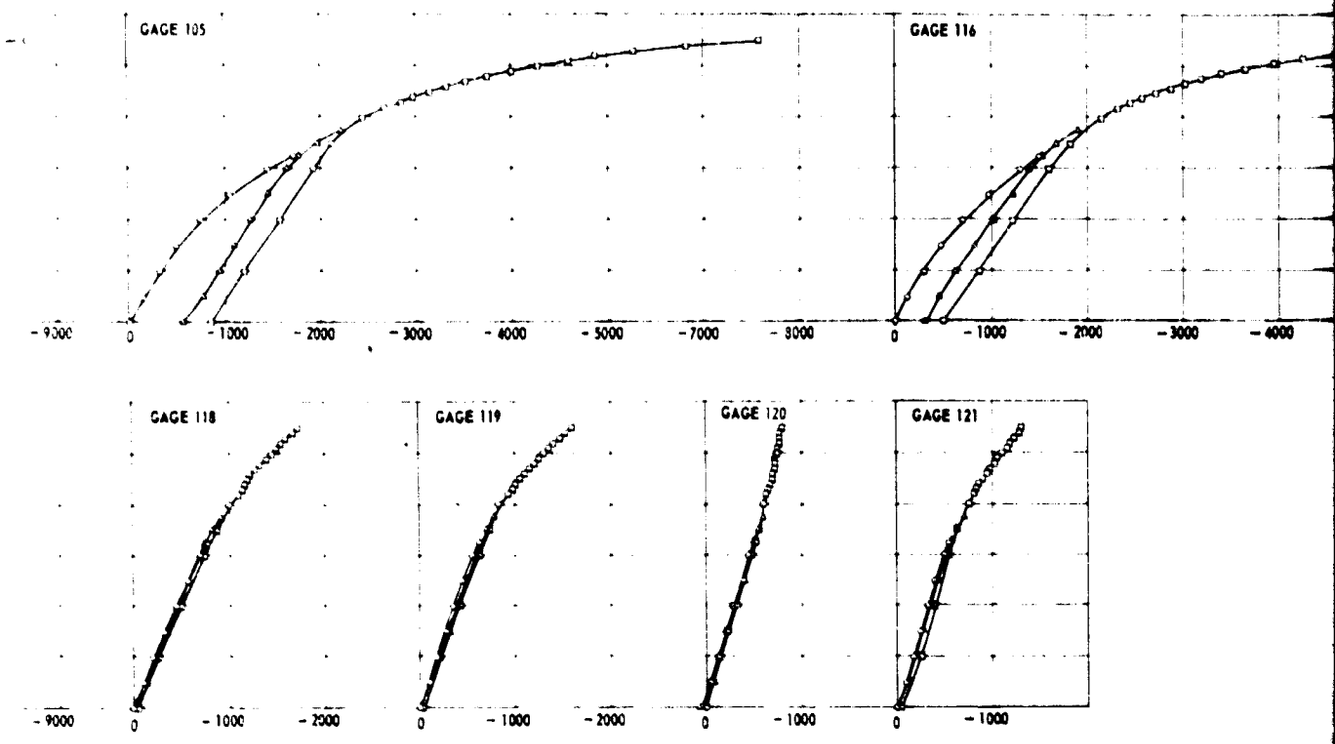
GAGE 115
GAGE 116
GAGE 118
GAGE 119
GAGE 120
GAGE 121
-9000
0
-1000
-2000
-3000
-4000
-5000
-7000
-8000

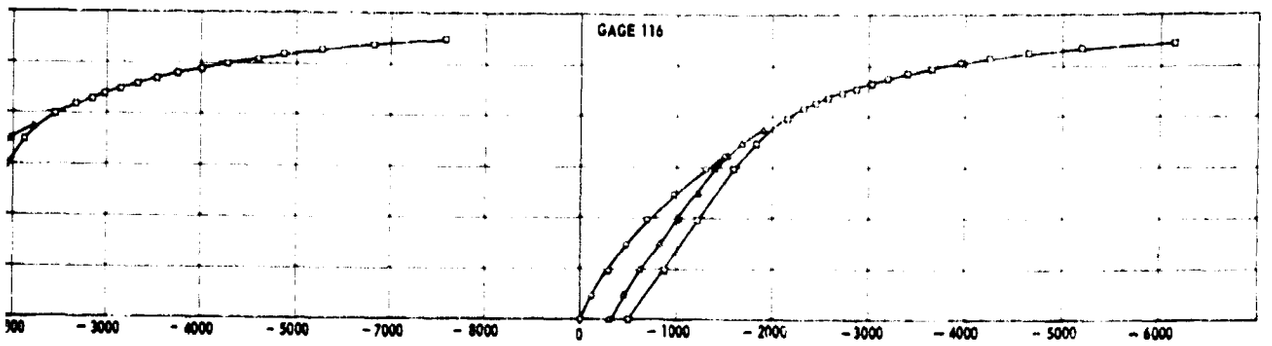
GAGE 116
- 3000
- 4000
- 5000
- 7000
- 8000
0
- 1000
- 2000
- 3000
- 4000
- 5000
- 6000

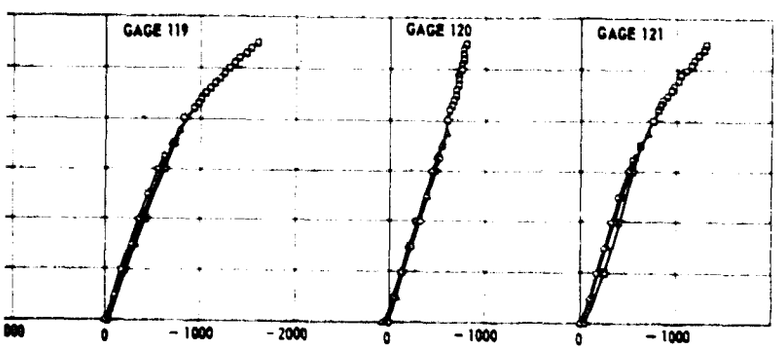
GAGE 119
GAGE 120
GAGE 121
0
- 1000
- 2000
0
- 1000
0
- 1000

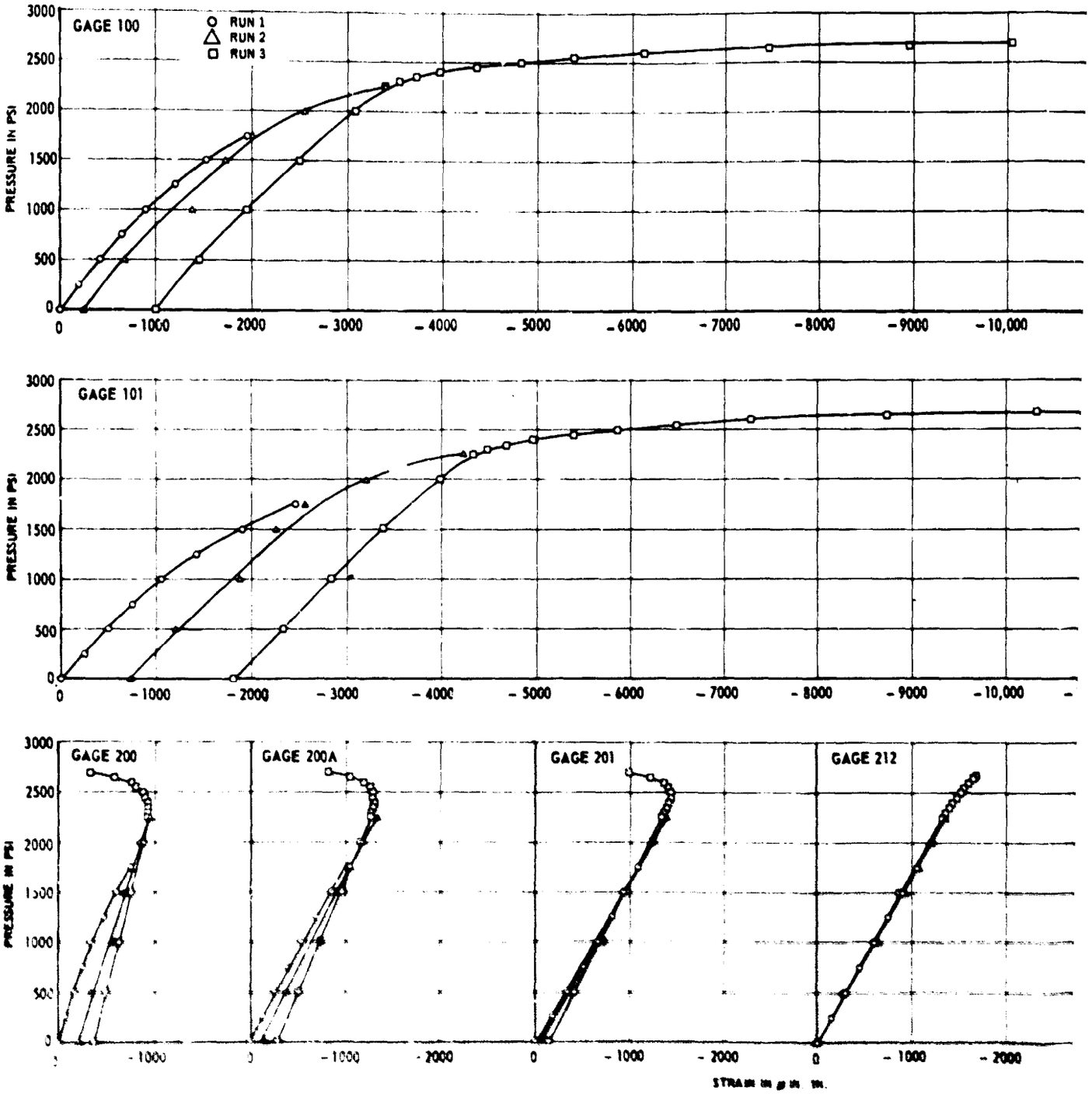
GAGE 100
RUN 1
RUN 2
RUN 3
PRESSURE IN PSI
3000
2500
2000
1500
1000
500
0
0
-1000
-2000
-3000
-4000
-5000
-6000
-7000
-8000
-9000
-10,000
GAGE 101
PRESSURE IN PSI
GAGE 200
GAGE 200A
GAGE 201
GAGE 212
PRESSURE IN PSI
STRAIN in μ in. in.

Figure 6

MODEL AF-3

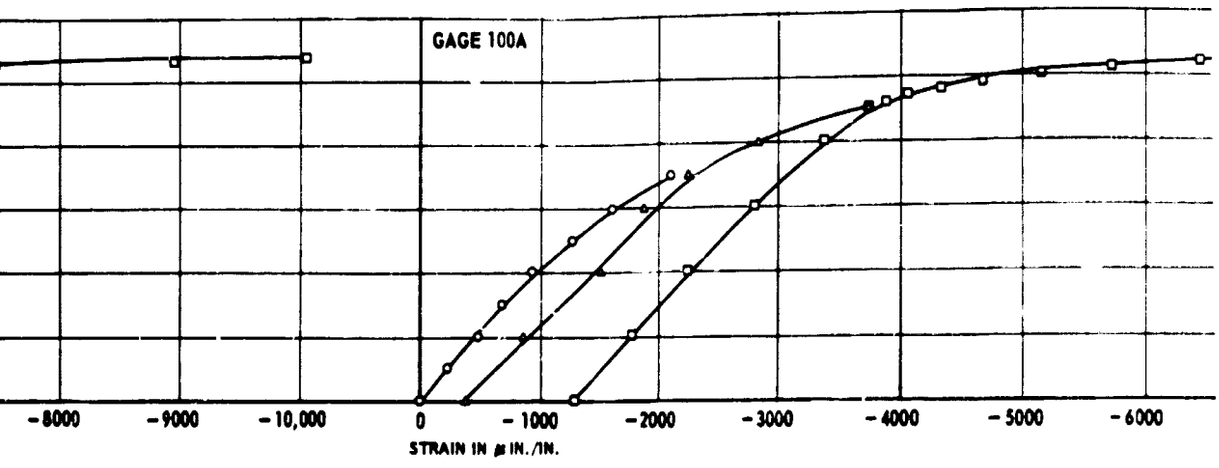

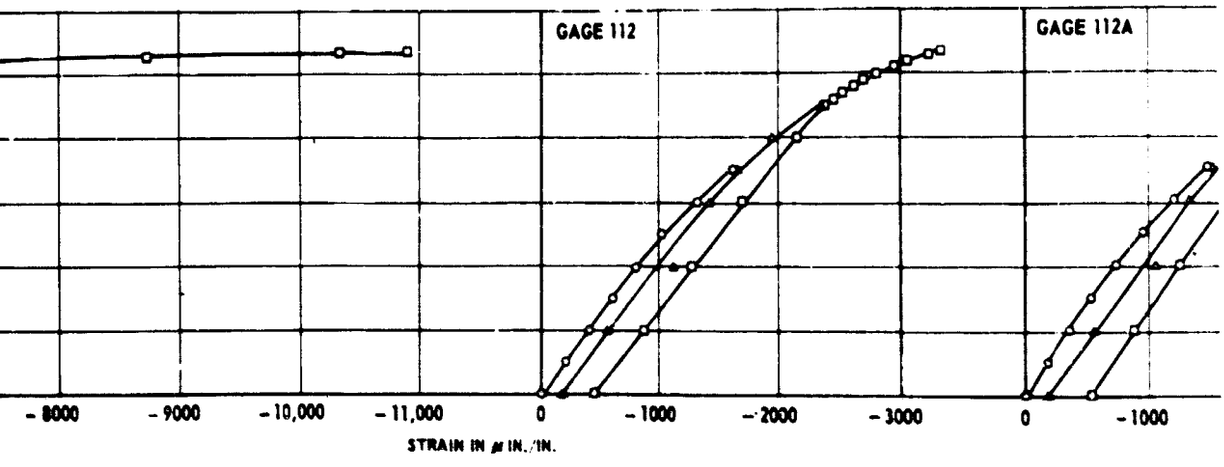

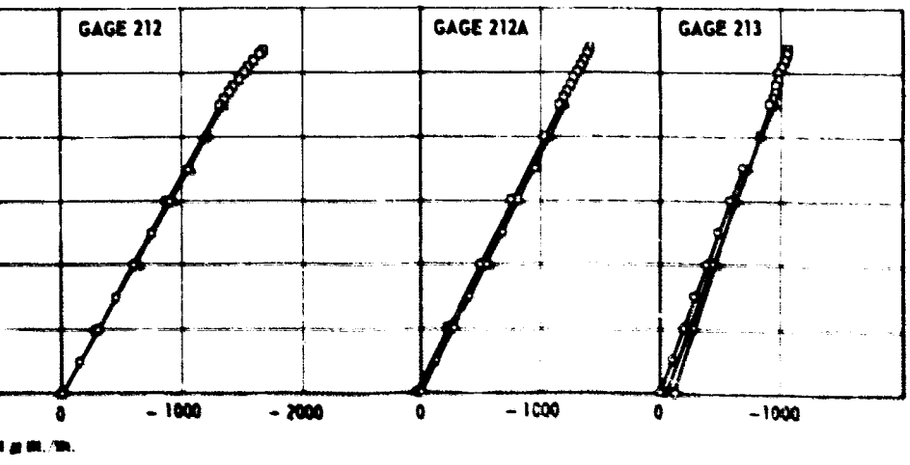

Figure 8c - Model AF-3

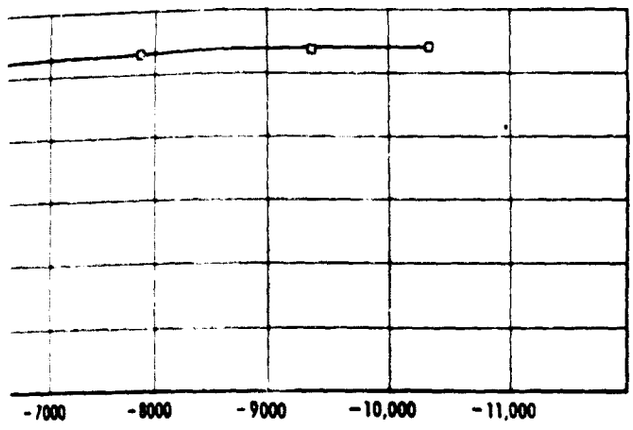
-7000
-8000
-9000
-10,000
-11,000

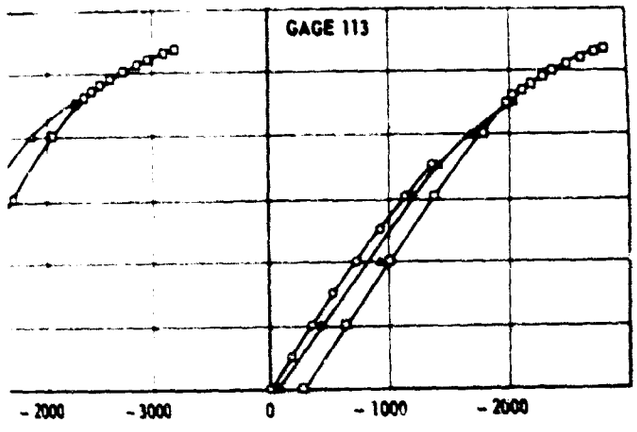
GAGE 113
-2000
-3000
0
-1000
-2000

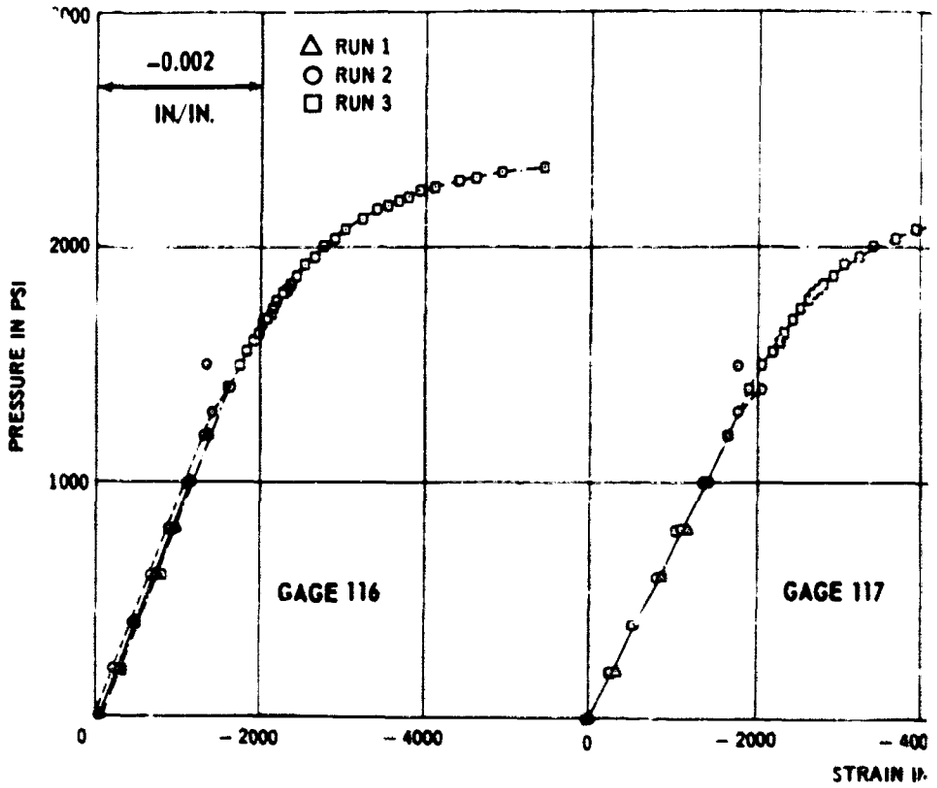
-0.002
IN/IN.
RUN 1
RUN 2
RUN 3
PRESSURE IN PSI
2000
1000
0
GAGE 116
GAGE 117
- 2000
- 4000
STRAIN IN

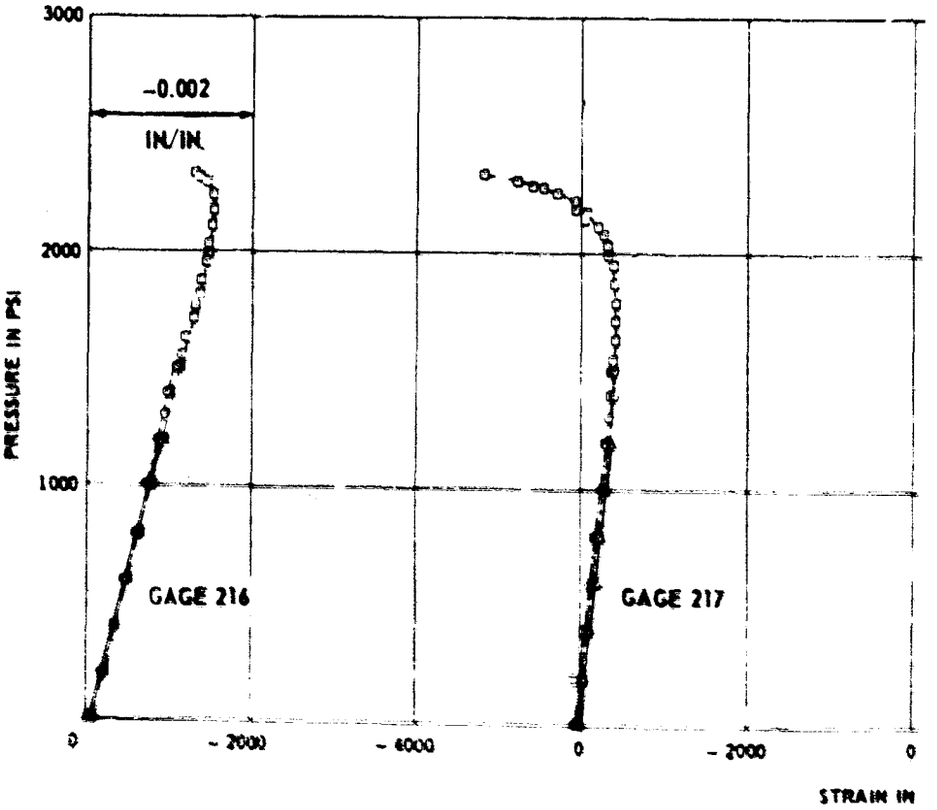
-0.002
IN/IN.
PRESSURE IN PSI
3000
2000
1000
0
GAGE 216
GAGE 217
- 2000
- 4000
STRAIN IN

Figure 8d -

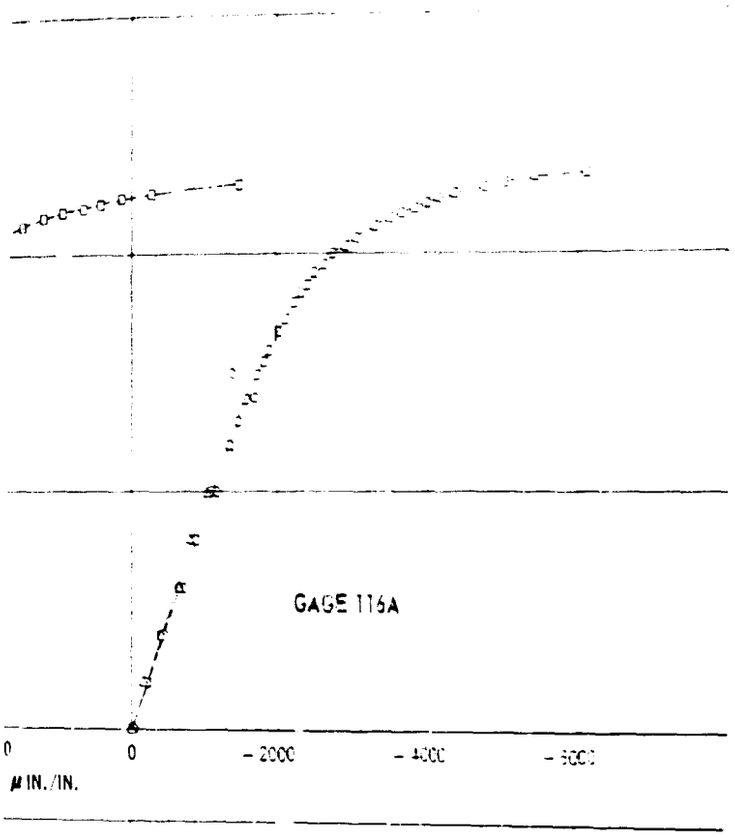

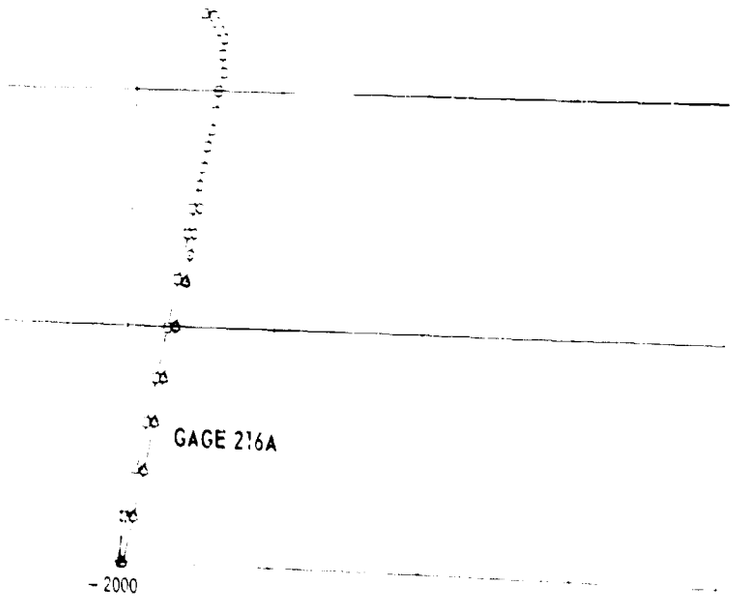

lode1 SRS-3

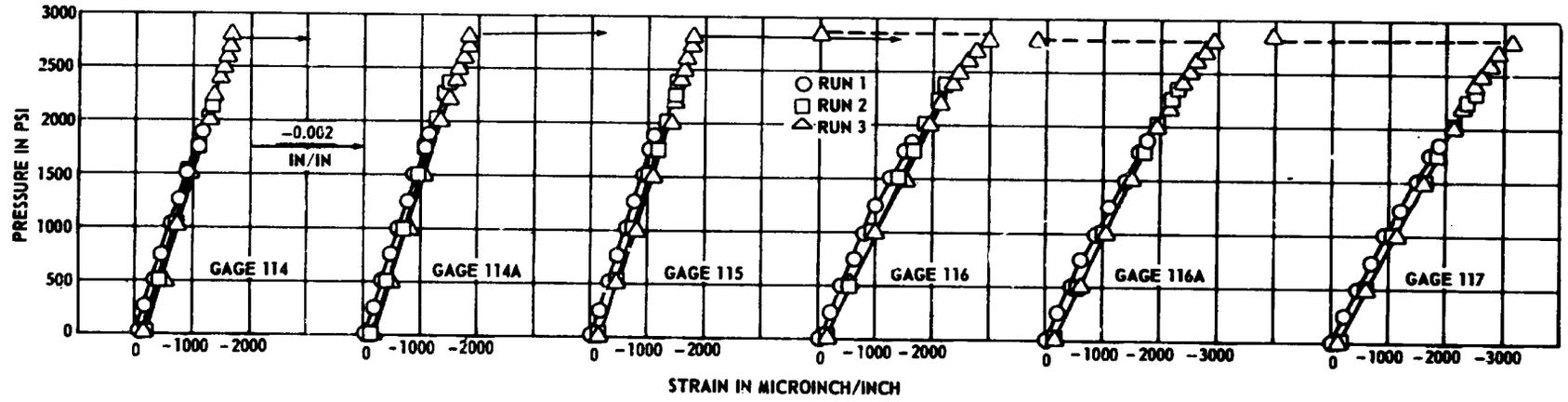

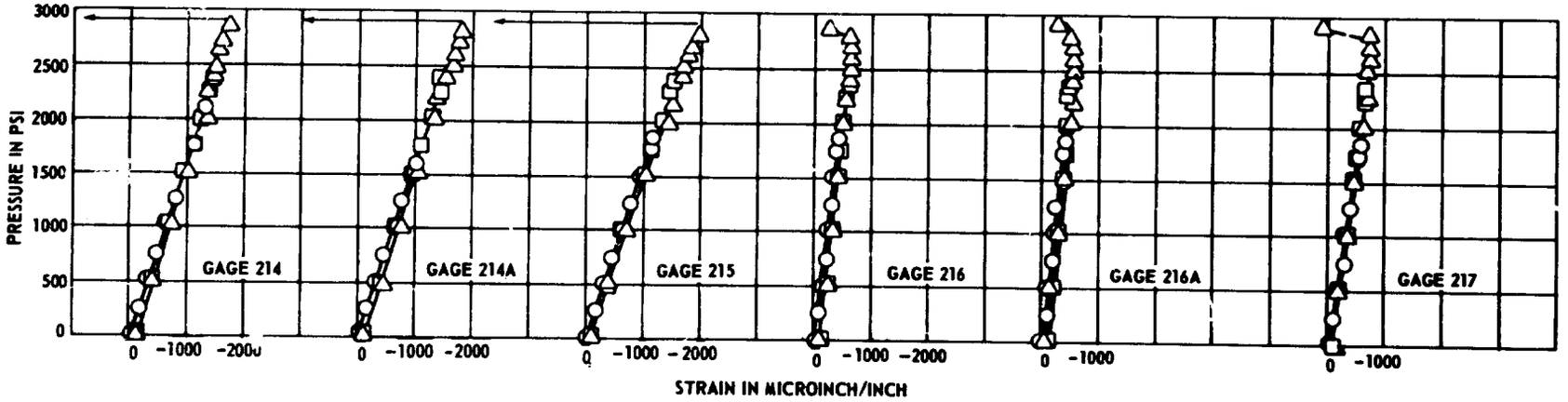

Figure 8e - Model SRS-4

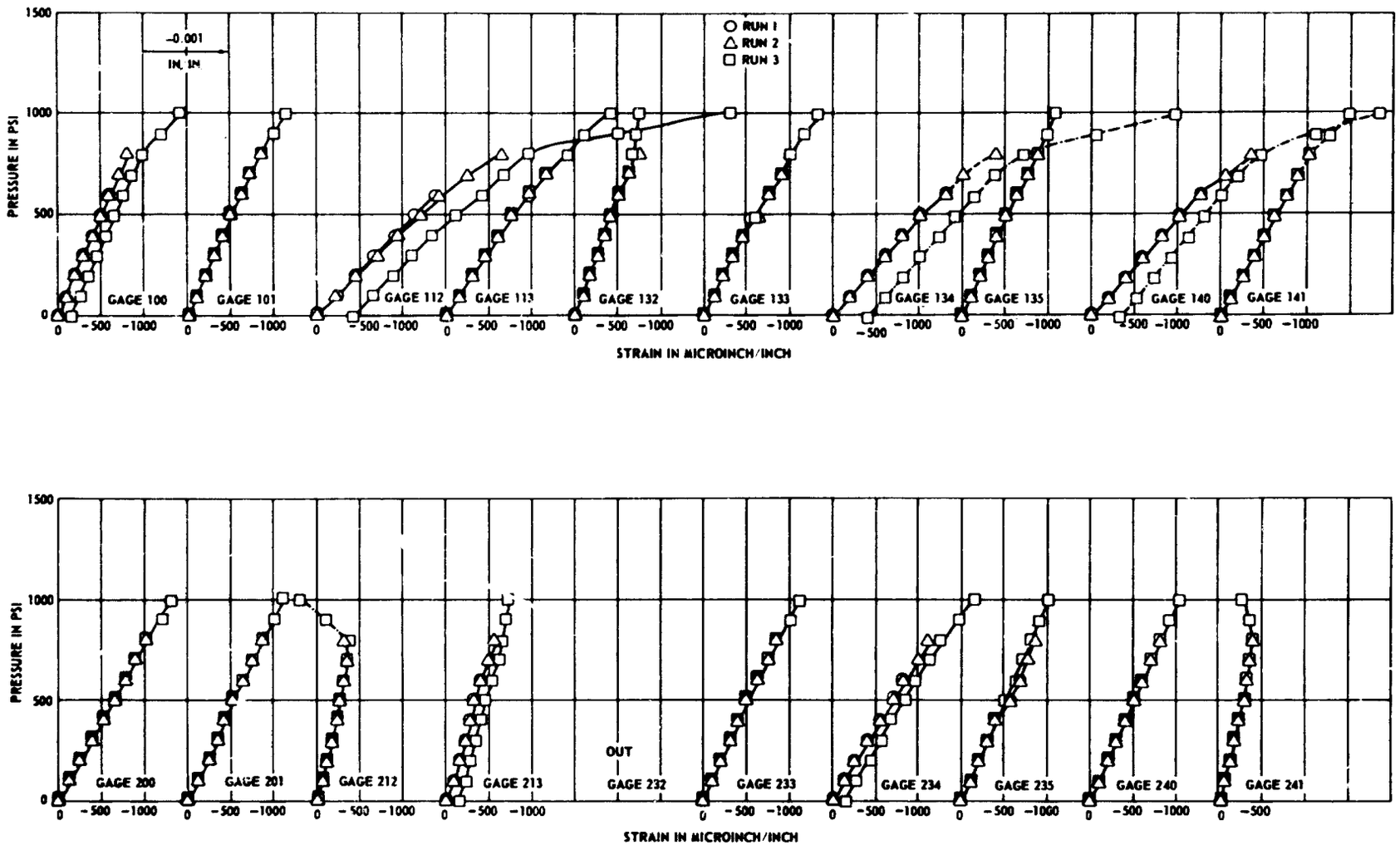

Figure 8f - Model SRS-2A

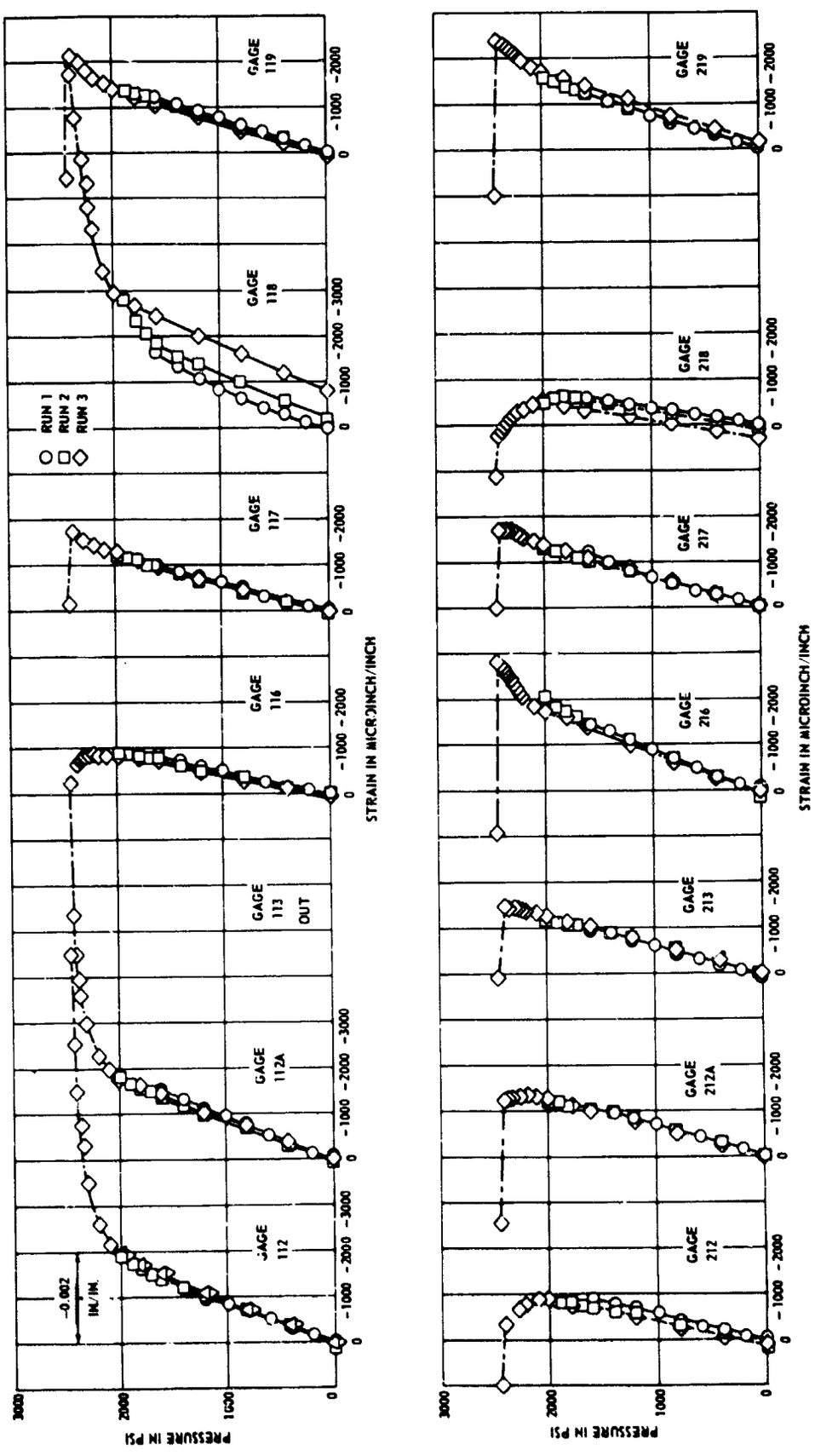

Figure 8g - Model SRS-3A

Figure 9 - Models After Collapse

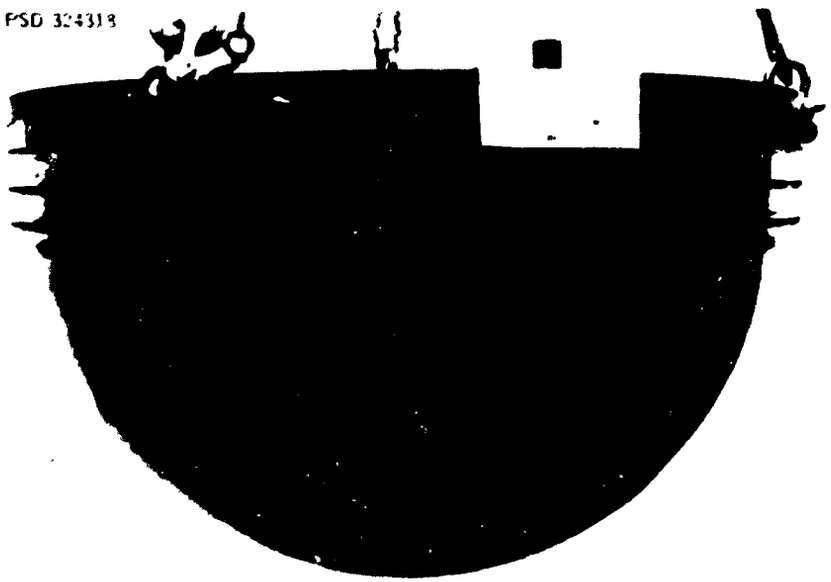

Figure 9a - Model AF-1

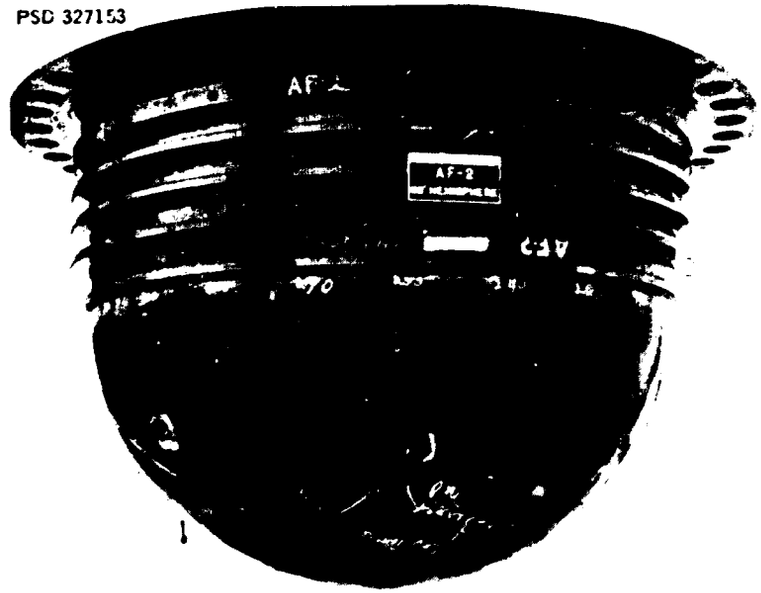

Figure 9b - Model AF-2

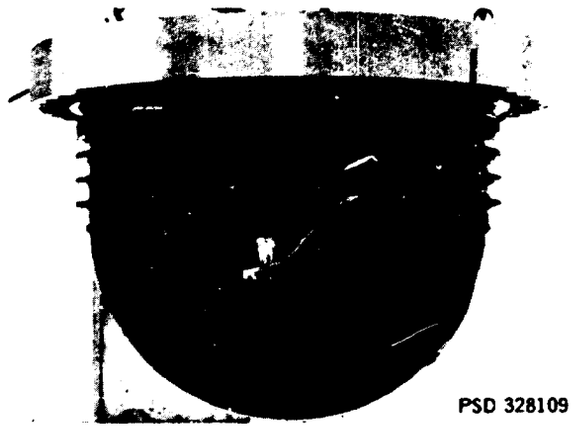

Figure 9c - Model AF-3

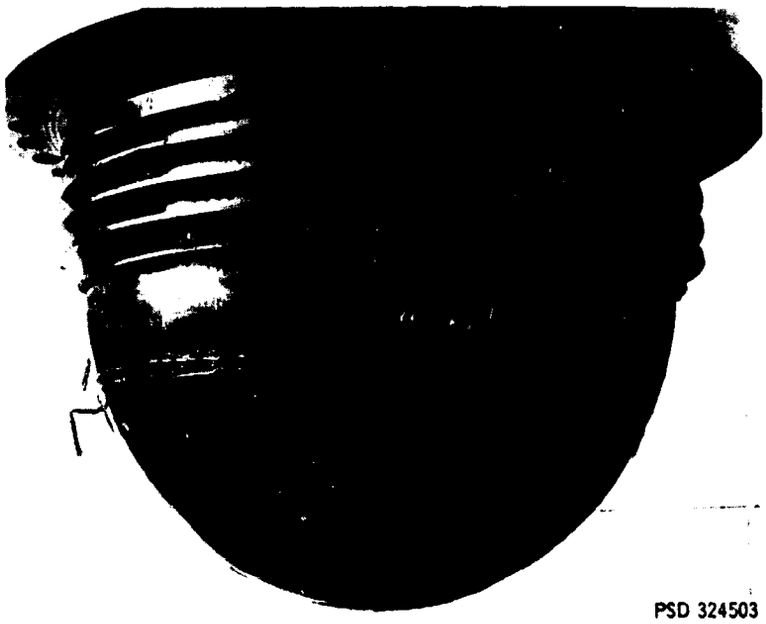

PSD 324503

Figure 9d - Model SRS-1

PSD 325446

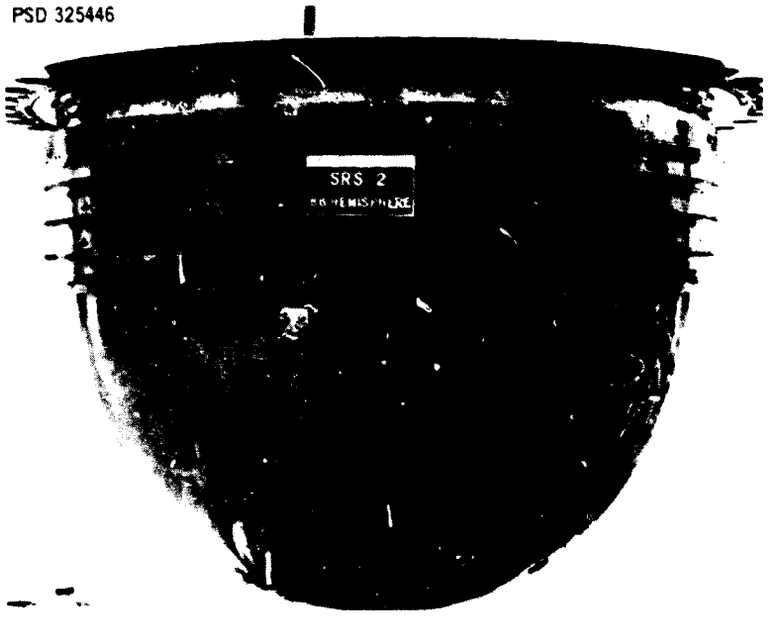

Figure 9e - Model SRS-2

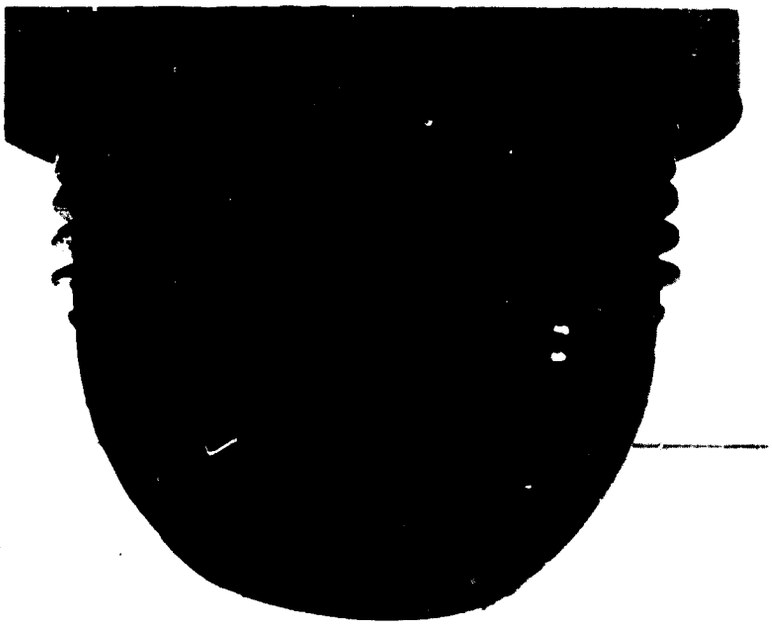

Figure 9f - Model SRS-3

Figure 9g - Model SRS-4

Figure 9h - Model SRS-2A

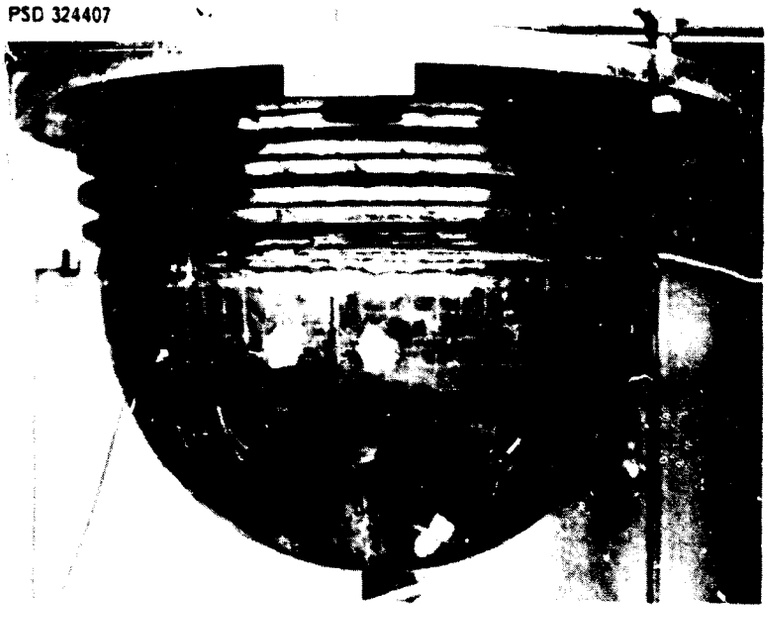

Figure 9i - Model SRS-3A

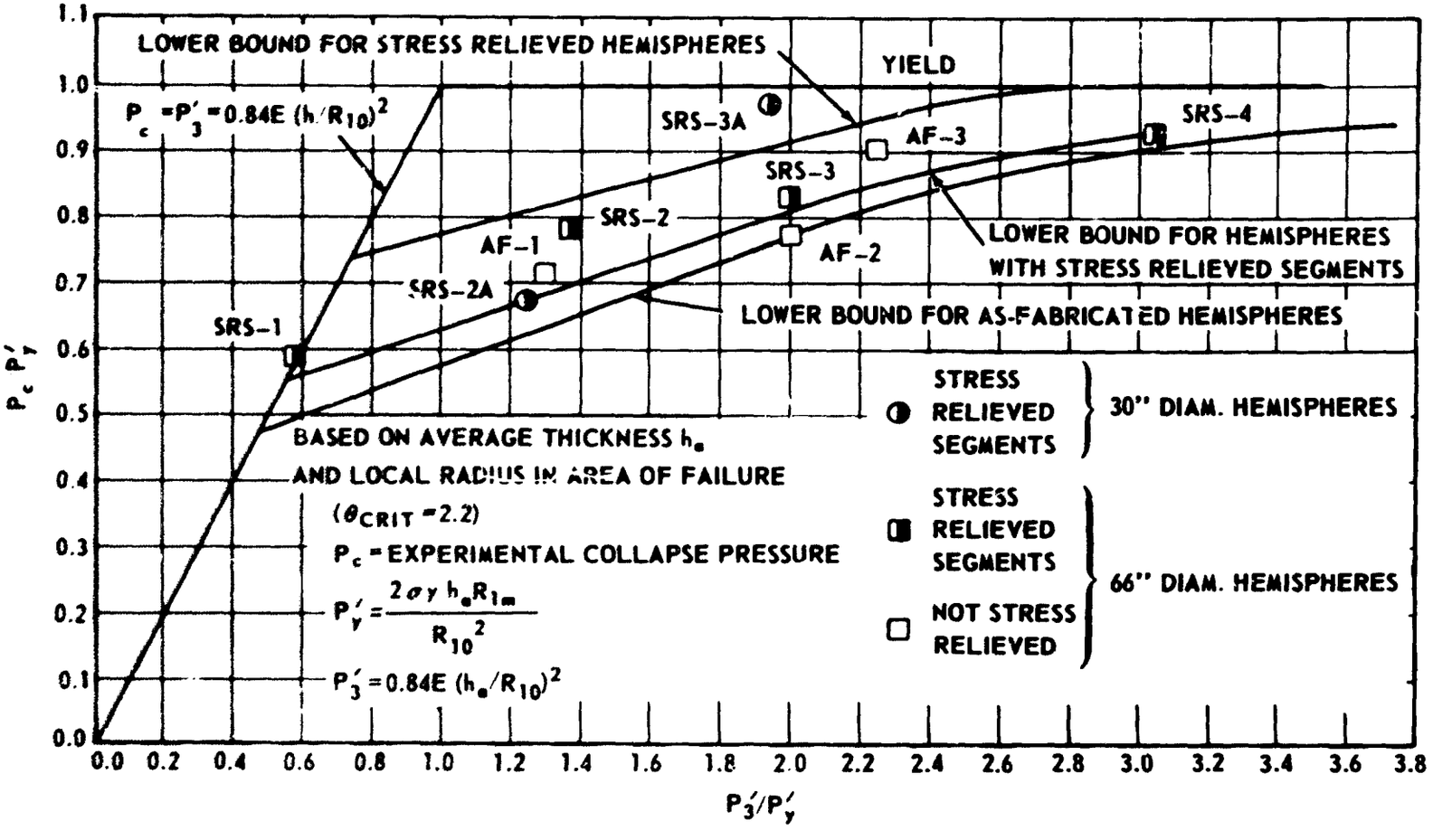

Figure 10 - Nondimensional Plot of Experimental Results for Fabricated HY-80 Steel Spherical Shells

TABLE 1

Compressive Yield Strengths

Model	Yield Strength in psi			
	Source of Yield Strength			
	Original Plate*	Coupon from Original Plate Stress Relieved with Model	Cold Formed Segment	Cold Formed and Stress Relieved Segment
AF-1	93,035			
AF-2	96,731			
AF-3	92,332			
SRS-1	95,951			
SRS-2	96,651	94,462		
SRS-3	95,453	94,789		
SRS-4	80,577			
SRS-2A	89,723		88,121	87,970
SRS-3A	90,830		90,117	90,417

*Used in calculations for P_y.

TABLE 2

Wall Thickness Readings

Meridional Orientation in degrees

Circumferential Orientation in degrees	0°	15	30	45	60°	75	90
0°	[illegible]	[illegible]	0.400	0.386	0.385	0.388	0.390	0.395
15		0.388	0.388	0.386			
30	0.395	0.396	0.395	0.385	0.385	0.397	0.392	
45		0.395	0.395	0.395			
60°	0.388	0.400	0.404	0.395	0.375	0.397	0.385	
60°	0.402	0.402	0.403	0.398	0.380			
75		0.395	0.395	0.395				
90	0.405	0.397	0.396	0.390	0.390	0.405	0.390	
105		0.397	0.396	0.395				
120°	0.396	0.403	0.404	0.399	0.380	0.409	0.391	
120°	0.398	0.398	0.396	0.410	0.390			
135		0.400	0.400	0.400				
150	0.407	0.399	0.396	0.395	0.381	0.396	0.388	
165	0.391	0.388	0.392					
180°	0.390	0.395	0.398	0.403	0.396	0.401	0.392	
180°	0.394	0.404	0.398	0.395	0.384			
195		0.394	0.394	0.396				
210	0.397	0.395	0.384	0.384	0.383	0.395	0.385	
225		0.386	0.391	0.390				
240°	0.401	0.406	0.402	0.395	0.380	0.392	0.385	
240°	0.393	0.393	0.400	0.404	0.384			
255		0.395	0.395	0.402				
270	0.402	0.392	0.391	0.394	0.385	0.396	0.386	
285		0.393	0.393	0.396				
300°	0.388	0.396	0.400	0.399	0.390	0.390	0.390	
300°	0.400	0.396	0.402	0.404	0.375			
315		0.391	0.394	0.400				
330	0.395	0.395	0.385	0.394	0.382	0.395	0.380	
345		0.385	0.390	0.395				
360°	0.390	0.390	0.403	0.398	0.380			

h_{AVG}=0.394 h_{MIN}=0.365 h_{MAX}=0.410

Model AF-1

Meridional Orientation in degrees

Circumferential Orientation in degrees	0°	15	30	45	60°	75	90
0°	0.629	0.628	0.628	0.628	0.614	0.612	0.605	0.605
15		0.620	0.611	0.602			
30	0.660	0.627	0.607	0.607	0.610	0.616	0.605	
45		0.621	0.611	0.621			
60°	0.629	0.618	0.624	0.620	0.615	0.617	0.600	
60°	0.630	0.615	0.630	0.628	0.619			
75		0.624	0.615	0.618				
90	0.645	0.619	0.619	0.614	0.616	0.624	0.608	
105		0.618	0.618	0.618				
120°	0.631	0.625	0.635	0.628	0.612	0.629	0.609	
120°	0.626	0.627	0.633	0.628	0.609			
135		0.619	0.609	0.611				
150	0.628	0.604	0.603	0.605	0.610	0.632	0.609	
165		0.618	0.610	0.618				
180°	0.625	0.626	0.632	0.622	0.609	0.631	0.618	
180°	0.627	0.622	0.626	0.625	0.622			
195		0.612	0.610	0.618				
210	0.628	0.602	0.603	0.608	0.618	0.629	0.609	
225		0.611	0.611	0.621				
240°	0.619	0.628	0.628	0.632	0.625	0.625	0.614	
240°	0.619	0.630	0.632	0.629	0.620			
255		0.612	0.620	0.617				
270	0.622	0.605	0.601	0.598	0.615	0.623	0.605	
285		0.605	0.608	0.610				
300°	0.611	0.610	0.620	0.616	0.605	0.620	0.605	
300°	0.621	0.630	0.628	0.631	0.624			
315		0.610	0.609	0.612				
330	0.615	0.608	0.595	0.609	0.625	0.611	0.605	
345		0.590	0.602	0.616				
360°	0.620	0.610	0.628	0.622	0.612	0.612	0.605	

h_{AVG}=0.618 h_{MIN}=0.590 h_{MAX}=0.660

Model AF-2

Table 4 (Continued)

Meridional Orientation in degrees

Circumferential Orientation in degrees	0°	15	30	45	60⁻	60⁺	75	90
0°	0.735	0.742	0.750	0.730	0.710	0.746	0.725	0.720
15		0.730	0.728	0.728				
30	0.750	0.738	0.712	0.727	0.745	0.725		
45		0.740	0.725	0.732				
60⁻	0.765	0.748	0.753	0.747	0.720	0.733	0.730	
60⁺	0.738	0.732	0.729	0.740	0.733			
75		0.729	0.735	0.737				
90	0.752	0.731	0.727	0.728	0.730	0.740	0.730	
105		0.730	0.725	0.732				
120⁻	0.745	0.732	0.749	0.749	0.727	0.745	0.730	
120⁺	0.742	0.735	0.744	0.756	0.741			
135		0.749	0.740	0.740				
150	0.780	0.758	0.726	0.734	0.740	0.745	0.728	
165		0.748	0.740	0.750				
180⁻	0.761	0.760	0.760	0.763	0.740	0.745	0.730	
180⁺	0.735	0.745	0.745	0.745	0.740			
195		0.739	0.739	0.740				
210	0.760	0.743	0.730	0.730	0.724	0.750	0.730	
225		0.732	0.730	0.726				
240⁻	0.739	0.740	0.745	0.745	0.735	0.754	0.735	
240⁺	0.740	0.745	0.750	0.741	0.730			
255		0.740	0.729	0.736				
270	0.748	0.735	0.715	0.724	0.735	0.760	0.740	
285		0.741	0.729	0.731				
300⁻	0.745	0.752	0.756	0.748	0.730	0.749	0.733	
300⁺	0.748	0.750	0.759	0.756	0.749			
315		0.745	0.740	0.740				
330	0.765	0.735	0.710	0.729	0.735	0.750	0.733	
345		0.729	0.720	0.733				
360⁻	0.730	0.735	0.745	0.750	0.732			

h_{AVG}=0.739 h_{MIN}=0.710 h_{MAX}=0.780

Model AF-1

Meridional Orientation in degrees

Circumferential Orientation in degrees	0°	15	30	45	60⁻	60⁺	75	90
0°	0.240	0.230	0.243	0.243	0.226	0.260	0.260	0.252
15		0.240	0.244	0.243				
30	0.243	0.242	0.244	0.243	0.230	0.253	0.258	
45		0.242	0.242	0.247				
60⁻	0.238	0.240	0.242	0.244	0.202	0.250	0.254	
60⁺	0.230	0.246	0.254	0.253	0.240			
75		0.239	0.252	0.254				
90	0.252	0.248	0.252	0.231	0.242	0.248	0.253	
105		0.255	0.257	0.255				
120⁻	0.246	0.244	0.246	0.246	0.230	0.247	0.254	
120⁺	0.255	0.256	0.256	0.250	0.228			
135		0.257	0.255	0.251				
150	0.251	0.255	0.255	0.253	0.228	0.256	0.262	
165		0.254	0.257	0.252				
180⁻	0.241	0.245	0.247	0.246	0.225	0.246	0.260	
180⁺	0.259	0.259	0.258	0.258	0.234			
195		0.258	0.255	0.252				
210	0.263	0.258	0.255	0.249	0.236	0.260	0.261	
225		0.256	0.256	0.252				
240⁻	0.256	0.254	0.248	0.252	0.231	0.260	0.260	
240⁺	0.250	0.242	0.254	0.254	0.234			
255		0.248	0.256	0.258				
270	0.253	0.254	0.250	0.258	0.246	0.265	0.260	
285		0.253	0.252	0.258				
300⁻	0.245	0.242	0.250	0.250	0.230	0.259	0.260	
300⁺	0.250	0.249	0.260	0.261	0.244			
315		0.251	0.256	0.256				
330	0.254	0.247	0.255	0.259	0.244	0.263	0.260	
345		0.241	0.257	0.258				
360⁻	0.240	0.228	0.244	0.256	0.237			

h_{AVG}=0.249 h_{MIN}=0.282 h_{MAX}=0.265

Model SRS-1

Table 2 (Continued)

Model SRS-2

Circumferential Orientation in degrees	Meridional Orientation in degrees: 0°	15	30	45	60⁻	60⁺	75	90
0°	0.381	0.386	0.390	0.381	0.376	0.364	0.386	0.369
15		0.382	0.386	0.382				
30	0.390	0.385	0.385	0.384	0.376	0.374	0.385	
45		0.385	0.390	0.392				
60⁻	0.378	0.384	0.391	0.381	0.379	0.375	0.380	
60°	0.380	0.375	0.383	0.390	0.365			
75		0.382	0.383	0.389				
90	0.384	0.376	0.380	0.386	0.370	0.360	0.386	
105		0.376	0.383	0.390				
120⁻	0.371	0.370	0.381	0.383	0.364	0.377	0.383	
120°	0.378	0.387	0.388	0.376	0.375			
135		0.386	0.390	0.390				
150	0.394	0.380	0.390	0.390	0.381	0.381	0.381	
165		0.384	0.388	0.389				
180⁻	0.380	0.375	0.387	0.385	0.376	0.381	0.387	
180°	0.383	0.390	0.385	0.380	0.372			
195		0.389	0.386	0.386				
210	0.394	0.390	0.387	0.385	0.373	0.366	0.390	
225		0.390	0.390	0.386				
240⁻	0.384	0.381	0.385	0.386	0.365	0.376	0.380	
240°	0.391	0.391	0.394	0.382	0.367			
255		0.387	0.390	0.385				
270	0.384	0.379	0.385	0.388	0.367	0.377	0.379	
285		0.392	0.394	0.386				
300⁻	0.385	0.372	0.390	0.280	0.364	0.360	0.384	
300°	0.390	0.390	0.392	0.389	0.365			
315		0.386	0.389	0.384				
330	0.391	0.385	0.384	0.381	0.361	0.370	0.382	
345		0.385	0.386	0.384				
360⁻	0.379	0.383	0.380	0.362	0.362			

h_{AVG}=0.381 h_{MIN}=0.360 h_{MAX}=0.396

Model SRS-3

Circumferential Orientation in degrees	Meridional Orientation in degrees: 0⁺	15	30	45	60⁻	60⁺	75	90
0⁺	0.620	0.610	0.660	0.650	0.620	0.640	0.650	0.600
15		0.640	0.650	0.660				
30	0.680	0.640	0.650	0.610	0.630	0.640	0.650	
45		0.640	0.650	0.650				
60⁻	0.640	0.680	0.680	0.640	0.610	0.650	0.650	
60⁺	0.650	0.650	0.680	0.680	0.620			
75		0.660	0.570	0.650				
90	0.690	0.660	0.660	0.640	0.640	0.650	0.650	
105		0.660	0.670	0.670				
120⁻	0.620	0.650	0.640	0.670	0.650	0.610	0.650	
120⁺	0.640	0.650	0.670	0.680	0.640			
135		0.640	0.650	0.650				
150	0.650	0.640	0.640	0.640	0.620	0.660	0.650	
165		0.640	0.650	0.650				
180⁻	0.640	0.660	0.680	0.680	0.680	0.650	0.650	
180⁺	0.670	0.670	0.680	0.680	0.690			
195		0.650	0.670	0.650				
210	0.670	0.660	0.650	0.620	0.640	0.630	0.640	
225		0.650	0.680	0.650				
240⁻	0.650	0.660	0.700	0.640	0.600	0.600	0.650	
240⁺	0.640	0.660	0.660	0.650	0.570			
255		0.660	0.670	0.650				
270	0.700	0.680	0.660	0.650	0.640	0.640	0.650	
285		0.670	0.660	0.660				
300⁻	0.640	0.640	0.640	0.580	0.600	0.600	0.650	
300⁺	0.640	0.640	0.670	0.640	0.620			
315		0.650	0.650	0.650				
330	0.690	0.650	0.650	0.620	0.640	0.640	0.640	
345		0.660	0.660	0.650				
360⁻	0.620	0.630	0.610	0.640	0.640			

h_{AVG}=0.649 h_{MIN}=0.580 h_{MAX}=0.700

Table 2 (Continued)

Meridional Orientation in degrees

Circumferential Orientation in degrees	0°	15	30	45	60⁻	60⁺	75	90
0°	0.721	0.733	0.746	0.737	0.714	0.742	0.731	0.724
15		0.730	0.732	0.735				
30	0.739	0.730	0.712	0.729	0.712	0.742	0.729	
45		0.725	0.729	0.723				
60⁻	0.721	0.723	0.698	0.729	0.702	0.738	0.732	
60°	0.735	0.735	0.735	0.731	0.719			
75		0.735	0.736	0.733				
90	0.741	0.734	0.730	0.731	0.715	0.734	0.732	
105		0.732	0.740	0.741				
120⁻	0.732	0.744	0.750	0.741	0.722	0.731	0.719	
120°	0.715	0.700	0.695	0.685	0.690			
135		0.722	0.720	0.710				
150	0.730	0.722	0.720	0.709	0.720	0.729	0.722	
165		0.722	0.722	0.722				
180⁻	0.718	0.712	0.721	0.709	0.698	0.740	0.729	
180°	0.714	0.727	0.740	0.741	0.700			
195		0.722	0.731	0.732				
210	0.739	0.730	0.721	0.728	0.712	0.720	0.726	
225		0.729	0.730	0.731				
240⁻	0.721	0.720	0.740	0.738	0.720	0.730	0.730	
240°	0.720	0.719	0.728	0.730	0.714			
255		0.730	0.729	0.712				
270	0.721	0.722	0.720	0.726	0.713	0.727	0.730	
285		0.725	0.725	0.729				
300⁻	0.718	0.732	0.730	0.731	0.709	0.735	0.730	
300°	0.731	0.740	0.730	0.739	0.734			
315		0.732	0.736	0.735				
330	0.741	0.730	0.723	0.732	0.715	0.743	0.735	
345		0.731	0.732	0.735				
360⁻	0.729	0.734	0.740	0.713				

h_{AVG}=0.726 h_{MIN}=0.685 h_{MAX}=0.750

Model SRS-4

Meridional Orientation in degrees

Circumferential Orientation in degrees	0⁺	15	30	45	60⁻	60⁺	75	90
0⁺	0.155	0.156	0.157	0.157	0.156	0.162	0.154	0.154
15		0.155	0.153	0.153				
30	0.158	0.159	0.152	0.153	0.156	0.161	0.154	
45		0.155	0.154	0.156				
60⁻	0.155	0.158	0.159	0.158	0.157	0.158	0.155	
60⁺	0.154	0.156	0.158	0.156	0.156			
75		0.156	0.157	0.154				
90	0.162	0.156	0.150	0.152	0.157	0.160	0.155	
105		0.157	0.154	0.155				
120⁻	0.159	0.159	0.161	0.158	0.157	0.160	0.154	
120⁺	0.156	0.159	0.160	0.159	0.159			
135		0.155	0.154	0.156				
150	0.158	0.154	0.154	0.156	0.161	0.160	0.154	
165		0.157	0.156	0.159				
180⁻	0.153	0.160	0.161	0.160	0.160	0.160	0.155	
180⁺	0.155	0.154	0.158	0.158	0.159			
195		0.156	0.154	0.157				
210	0.158	0.152	0.150	0.154	0.159	0.161	0.154	
225		0.155	0.154	0.157				
240⁻	0.153	0.156	0.157	0.158	0.159	0.162	0.154	
240⁺	0.159	0.160	0.163	0.162	0.162			
255		0.159	0.158	0.158				
270	0.162	0.158	0.155	0.157	0.163	0.162	0.155	
285		0.160	0.158	0.161				
300⁻	0.159	0.161	0.163	0.163	0.162	0.161	0.155	
300⁺	0.160	0.162	0.164	0.160	0.160			
315		0.161	0.159	0.159				
330	0.162	0.160	0.156	0.157	0.161	0.155		
345		0.161	0.158	0.159				
360⁻	0.160	0.162	0.162	0.161	0.161			

h_{AVG}=0.158 h_{MIN}=0.150 h_{MAX}=0.164

Model SRS-2A

Table 2 (Continued)

Meridional Orientation in degrees

Circumferential Orientation in degrees	0^+	15	30	45	60^-	60^+	75	90
0^+	0.252	0.251	0.252	0.251	0.251	0.251	0.244	0.242
15		0.247	0.242	0.244				
30	0.244	0.242	0.240	0.244	0.248	0.251	0.244	
45		0.243	0.242	0.244				
60^-	0.250	0.250	0.240	0.249	0.250	0.252	0.243	
60^+	0.252	0.251	0.252	0.251	0.254			
75		0.247	0.246	0.247				
90	0.254	0.246	0.240	0.240	0.250	0.250	0.244	
105		0.247	0.244	0.244				
120^-	0.252	0.250	0.250	0.251	0.249	0.250	0.243	
120^+	0.250	0.250	0.250	0.247	0.248			
135		0.245	0.242	0.243				
150	0.254	0.242	0.240	0.240	0.246	0.251	0.243	
165		0.243	0.242	0.241				
180^-	0.250	0.250	0.248	0.249	0.249	0.254	0.243	
180^+	0.249	0.248	0.251	0.250	0.251			
195		0.244	0.246	0.244				
210	0.252	0.244	0.240	0.243	0.252	0.256	0.244	
225		0.247	0.242	0.244				
240^-	0.247	0.247	0.248	0.248	0.248	0.251	0.244	
240^+	0.252	0.250	0.250	0.249	0.250			
255		0.247	0.243	0.244				
270	0.254	0.244	0.240	0.241	0.247	0.249	0.244	
285		0.247	0.242	0.241				
300^-	0.251	0.250	0.249	0.250	0.251	0.252	0.245	
300^+	0.252	0.253	0.250	0.248	0.249			
315		0.249	0.251	0.247				
330	0.251	0.244	0.246	0.240	0.247	0.249	0.245	
345		0.246	0.240	0.241				
360^-	0.251	0.249	0.250	0.250	0.248			

h_{AVG}=0.247 h_{MIN}=0.240 h_{MAX}=0.256

Model SRS-3A

TABLE 3

Local Geometry and Comparison of Calculated and Measured Membrane Stresses and Collapse Pressures

Model	Area	h_a inch	$\frac{R_1}{R}$	Calculated Max. Memb. Stress Sens.[1] psi/psi	Measured Max. Memb. Stress Sens.[2] psi/psi	Ratio of Calc. to Meas. Stress	Exp. Collapse Pressure, psi
AF-1	I	0.395	1.32	55.72	50.67	1.100	1260
	II*	0.391	1.23	52.50	53.14	0.988	
	III	0.393	1.23	52.23	50.27	1.039	
	IV	0.390	1.19	50.94	51.15	0.996	
	V	0.398	1.18	49.52	47.01	1.053	

	I	0.623	1.32	35.65	33.55	1.063	
	II	0.630	1.26	33.70	33.50	1.006	
AF-2	III	0.615	1.26	34.50	31.68	1.089	2240
	IV	0.609	1.25	34.56	28.10	1.229	
	V	0.629	1.23	32.96	31.90	1.033	
	VI*	0.627	1.23	33.07	31.60	1.047	
	I*	0.724	1.32	30.78	33.11	0.929	
	II	0.728	1.26	29.26	29.70	0.985	
AF-3	III	0.730	1.22	28.28	29.44	0.961	2700
	IV	0.728	1.20	27.90	29.54	0.944	
	V	0.722	1.19	27.90	30.69	0.909	
	I*	0.252	1.76	115.50	111.4	1.037	
	II	0.250	1.25	82.90	84.5	0.981	
SRS-1	III	0.255	1.24	80.64	77.4	1.042	490
	IV	0.252	1.23	80.95	80.5	1.006	
	V	0.243	1.19	80.21	92.0	0.872	
	I	0.389	1.20	51.34	gage out	---	
	II	0.385	1.20	51.87	50.42	1.028	
SRS-2	III	0.389	1.19	50.93	50.68	1.005	1575
	IV	0.390	0.17	49.96	gage out	---	
	V	0.381	1.15	50.26	50.17	1.002	
	VI*	0.387	1.11	47.80	no gage	---	
	I	0.620	1.36	36.85	32.69	1.127	
	II	0.655	1.34	34.42	35.96	0.957	
SRS-3	III*	0.620	1.23	33.40	36.80	0.908	2360
	IV	0.660	1.19	30.42	34.00	0.895	
	V	0.660	1.17	29.93	36.22	0.826	
	I	0.733	1.39	31.95	26.06	1.226	
	II	0.737	1.32	30.22	26.34	1.147	
SRS-4	III	0.726	1.20	27.94	26.18	1.067	2850
	IV	0.721	1.17	27.45	26.25	1.046	
	V	0.724	1.16	27.11	25.85	1.049	
	VI*	0.724	1.12	26.20	24.97	1.049	
				65.43	56.79	1.152	

	IV	0.660	1.19	30.42	34.00	0.895	
	V	0.660	1.17	29.93	36.22	0.826	
SRS-4	I	0.733	1.39	31.95	26.06	1.226	2850
	II	0.727	1.32	30.22	26.34	1.147	
	III	0.726	1.20	27.94	26.18	1.067	
	IV	0.721	1.17	27.45	26.25	1.046	
	V	0.724	1.16	27.11	25.85	1.049	
	VI*	0.724	1.12	26.20	24.97	1.049	
SRS-2A	I	0.157	1.36	65.43	56.79	1.152	1060
	II	0.160	1.27	59.39	59.59	0.997	
	III	0.155	1.27	62.27	51.95	1.199	
	IV	0.160	1.22	57.96	gage out	---	
	V	0.157	1.21	58.21	57.79	1.007	
	VI*	0.156	1.17	56.96	no gage	---	
SRS-3A	I*	0.248	1.17	36.09	gage out	---	2440
	II	0.247	1.13	35.00	31.32	1.117	
	III	0.248	1.13	34.86	31.74	1.098	
	IV	0.247	1.10	34.08	32.75	1.041	
	V	0.249	1.10	33.81	31.45	1.075	

1. The calculated stress sensitivities are determined from the equation

$$\text{Stress sensitivity} = \frac{R_{10}^{\,2}}{2\, h_a\, R_{1m}}$$

2. The measured stress sensitivities are based on the average of the strain-sensitivity readings taken on the inside and outside surfaces of the shell. The strain sensitivity is defined as the slope of the portion of the pressure-strain diagram which is linear. Measured stress sensitivities are determined from the expression

$$\text{Stress sensitivity} = \frac{E}{0.2}\left[\frac{\varepsilon_1+\varepsilon_3}{1-\mu} + \frac{1}{1+\mu}\sqrt{\left(\varepsilon_1-\varepsilon_3\right)^2 + \left[2\varepsilon_2 - \left(\varepsilon_1+\varepsilon_3\right)^2\right]}\right]$$

where ε_1, ε_2, and ε_3 are the average strain sensitivities at the 0-, 45-, and 90-deg orientation in a three-element rosette.

*Failure area.

TABLE 4

Comparison of Predicted and Experimental Collapse Pressures

Model	Failure Area	P_{pred}^*	P_{exp}	$\frac{P_{exp}}{P_{pred}}$
AF-1	II	1035	1260	1.22
AF-2	VI	2076	2240	1.08
AF-3	I	2460	2700	1.10
SRS-1	I	465	490	1.04
SRS-2	VI	1280	1575	1.23
SRS-3	III	2007	2360	1.18
SRS-4	VI	2207	2850	1.29
SRS-2A	VI	880	1060	1.20
SRS-3A	I	2001	2440	1.22

*P_{pred} is determined by calculating P_j and P_y at Area I, the "critical" area with respect to h_a/R_1, and then using the proper lower bound curve in Figure 10 to get P_c or P_{pred}. The data points in Figure 10 were based on the local geometry in the "failure area."

REFERENCES

1. Kiernan, T.J. and Nishida, K., "The Buckling Strength of Fabricated HY-80 Steel Spherical Shells," David Taylor Model Basin Report 1721 (Jul 1966).

2. Costello, M.G. and Nishida, K., "The Inelastic Buckling Strength of Fabricated HY-80 Steel Hemispherical Shells," NSRDC Report 2304 (Apr 1967).

3. Krenzke, M.A. and Kiernan, T.J., "The Effect of Initial Imperfections on the Collapse Strength of Deep Spherical Shells," David Taylor Model Basin Report 1757 (Feb 1965).

4. Costello, M.G., "The Effect of Mismatch on the Collapse Strength of Machined Hemispherical Shells," NSRDC Report 3383 (Jul 1970).

UNCLASSIFIED
Security Classification

DOCUMENT CONTROL DATA - R & D

(Security classification of title, body of abstract and indexing annotation must be entered when the overall report is classified)

1. ORIGINATING ACTIVITY (Corporate author)

Naval Ship Research and Development Center
Washington, D. C. 20034

2a. REPORT SECURITY CLASSIFICATION
Unclassified

2b. GROUP

3. REPORT TITLE

THE EFFECT OF RESIDUAL STRESSES ON THE BUCKLING STRENGTH OF FABRICATED HY-80 STEEL HEMISPHERICAL SHELLS

4. DESCRIPTIVE NOTES (Type of report and inclusive dates)

Final Report

5. AUTHOR(S) (First name, middle initial, last name)

M. G. Costello

6. REPORT DATE	7a. TOTAL NO. OF PAGES	7b. NO. OF REFS
October 1970	54	4

8a. CONTRACT OR GRANT NO	9a. ORIGINATOR'S REPORT NUMBER(S)
b. PROJECT NO SF 35.422.210, Task 15054	
c.	9b. OTHER REPORT NO(S) (Any other numbers that may be assigned this report)
d.	

10. DISTRIBUTION STATEMENT

This document is subject to special export controls and each transmittal to foreign governments or foreign nationals may be made only with prior approval of Naval Ship Research and Development Center, Code 700.

11. SUPPLEMENTARY NOTES	12. SPONSORING MILITARY ACTIVITY
	Naval Ship Systems Command

13. ABSTRACT

Hydrostatic tests were conducted on nine fabricated HY-80 steel hemispheres to observe the effects of residual stresses from cold forming and welding on elastic response and collapse strength. Non-dimensionalized collapse data indicated that residual stresses due to welding play a significant part in the collapse strength of fabricated HY-80 steel hemispheres.

DD FORM 1473 (PAGE 1)

S/N 0101-807-6801

UNCLASSIFIED
Security Classification

12

14 KEY WORDS	LINK A		LINK B		LINK C	
	ROLE	WT	ROLE	WT	ROLE	WT
Spherical Shells						
Initial Imperfections						
Residual Stresses						
Buckling						
Elastic Behavior						
Inelastic Behavior						